

A wide deep infrared look at the Pleiades with UKIDSS: new constraints on the substellar binary fraction and the low mass IMF ^{*}

N. Lodieu^{1,2,†}, P. D. Dobbie^{3,2}, N. R. Deacon⁴, S. T. Hodgkin⁵, N. C. Hambly⁶,
R. F. Jameson²

¹*Instituto de Astrofísica de Canarias, Vía Láctea s/n, E-38205 La Laguna, Tenerife, Spain*

²*Department of Physics and Astronomy, University of Leicester, University Road, Leicester LE1 7RH, UK*

³*Anglo-Australian Observatory, PO Box 296, Epping, NSW, 1710, Australia*

⁴*Department of Astrophysics, Radboud University Nijmegen, P.O. Box 9010, 6500 GL Nijmegen, The Netherlands*

⁵*Institute of Astronomy, Madingley Road, Cambridge CB3 0HA*

⁶*Scottish Universities' Physics Alliance (SUPA), Institute for Astronomy, School of Physics, University of Edinburgh, Royal Observatory, Blackford Hill, Edinburgh EH9 3HJ, UK*

Accepted 31 October 2021. Received 31 October 2021; in original form 31 October 2021

ABSTRACT

We present the results of a deep wide-field near-infrared survey of 12 square degrees of the Pleiades conducted as part of the UKIDSS Deep Infrared Sky Survey (UKIDSS) Galactic Cluster Survey (GCS). We have extracted over 340 high probability proper motion members down to 0.03 solar masses (M_{\odot}) using a combination of UKIDSS photometry and proper motion measurements obtained by cross-correlating the GCS with data from the Two Micron All Sky Survey (2MASS), the Isaac Newton (INT) and the Canada-France-Hawai'i (CFHT) telescopes. Additionally, we have unearthed 73 new candidate brown dwarf members on the basis of five band UKIDSS photometry alone. We have identified 23 substellar multiple system candidates out of 63 candidate brown dwarfs from the $(Y-K, Y)$ and $(J-K, J)$ colour-magnitude diagrams, yielding a binary frequency of 28–44% in the 0.075–0.030 M_{\odot} mass range. Our estimate is three times larger than the binary fractions reported from high-resolution imaging surveys of field ultracool dwarfs and Pleiades brown dwarfs. However, it is marginally consistent with our earlier “peculiar” photometric binary fraction of $50 \pm 10\%$ presented in Pinfield et al. (2003), in good agreement with the 32–45% binary fraction derived from the recent Monte-Carlo simulations of Maxted & Jeffries (2005) and compatible with the $26 \pm 10\%$ frequency recently estimated by Basri & Reiners (2006). A tentative estimate of the mass ratios from photometry alone seems to support the hypothesis that binary brown dwarfs tend to reside in near equal-mass ratio systems. In addition, the recovery of four Pleiades members targeted by high-resolution imaging surveys for multiplicity studies suggests that half of the binary candidates may have separations below the resolution limit of the *Hubble Space Telescope* or current adaptive optics facilities at the distance of the Pleiades ($a \sim 7$ AU). Finally, we have derived luminosity and mass functions from the sample of photometric candidates with membership probabilities. The mass function is well modelled by a log-normal peaking at 0.24 M_{\odot} and is in agreement with previous studies in the Pleiades.

Key words: Techniques: photometric — stars: low-mass, brown dwarfs; stars: luminosity function, mass function — galaxy: open clusters and associations: individual (Pleiades) — infrared: stars

1 INTRODUCTION

Over the past two decades star forming regions and rich, young open clusters have been the focal points of numerous searches for substellar objects (e.g. Jameson & Skillen 1989; Luhman 1999; Lucas & Roche 2000; Béjar et al. 2001; Moraux et al. 2003; Lodieu et al. 2006, 2007). Part of the reasoning behind this is that in these environments brown dwarfs (BDs), which cool and fade af-

* Based on observations made with the United Kingdom Infrared Telescope, operated by the Joint Astronomy Centre on behalf of the U.K. Particle Physics and Astronomy Research Council.

† E-mail: nlodieu@iac.es

ter a brief period of deuterium burning ($\sim 2\text{--}20$ Myr; Baraffe et al. 1998; Palla & Baraffe 2005), are comparatively luminous, allowing 2/4m class telescopes to probe to very low-masses. Furthermore, the members of such an agglomeration likely have a common age, distance and composition making a theoretical interpretation of their observed properties somewhat more straightforward (e.g. mass estimates). The ultimate aim of these deep surveys is to characterise the substellar population, including the relative numbers of members as a function of mass, the lower mass limit to their manufacture, the binary fraction and the spatial distribution. Observational constraints on these properties can be used to critically examine models of the star formation process. Furthermore, comparison of these properties as derived in a number of different environments can provide clues as to whether the Initial Mass Function (IMF; dN/dm) and the binary fraction, as a function of mass, are universal or dependent on the conditions in the nascent molecular clouds (Briceño et al. 2002; Luhman 2004).

The rich Pleiades cluster has been subjected to a particularly high degree of scrutiny as it has a number of highly attractive properties. For example, its constituents share a sizeable common proper motion ($\mu_\alpha \cos \delta = 19.15$ and $\mu_\delta = -45.72$ mas/yr; Robichon et al. 1999) so it is relatively straightforward to discriminate members from the general field star population. The distance and the age of the cluster are well constrained. Estimates of the former, which includes a meticulous astrometric analysis of the binary Atlas, concentrate around 134 pc with an uncertainty of 5 pc (Johnson 1957; Gatewood et al. 2000; Pinfield et al. 2000; Southworth et al. 2005). The latter is estimated to be 125 ± 8 Myrs based on the location of the “lithium boundary” (Rebolo, Martín & Magazzù 1992) as observed in the spectra of low-mass members (Stauffer et al. 1998). Additionally, reddening along the line of sight to the cluster is generally low, $E(B - V) = 0.03$ (O’dell, Hendry & Collier Cameron 1994).

Recent work on very young clusters (age < 10 Myrs) and star-formation regions e.g. σ Ori (Béjar et al. 2001), the Trapezium Cluster (Muench et al. 2002; Slesnick et al. 2004), IC348 (Luhman et al. 1998, 2000; Muench et al. 2003), Upper Sco (Lodieu et al. 2007) suggests that the IMF continues slowly rising, down to about $m=0.01M_\odot$, at least in these environments. However, mass estimates of young BDs (age around 1 Myr or less) derived from the direct comparison of their observed properties to the predictions of theoretical models should be treated with caution because evolutionary calculations are not yet coupled to detailed simulations of the collapse and accretion phase of star formation (Baraffe et al. 2002). Similarly, Hillenbrand & White (2004) showed that models tend to underestimate masses by a few tens of percent in the $m = 1.0\text{--}0.3 M_\odot$ mass range from an analysis of available dynamical mass measurements of pre-main-sequence stars. While it would be imprudent to claim that the interpretation of observational data related to members of the Pleiades is completely free of such uncertainties, given the greater maturity of the cluster it seems realistic to assume that these uncertainties are significantly reduced.

Previous CCD based studies of the Pleiades indicate that the present day mass function, across the stellar/substellar boundary and down to $m\sim 0.03M_\odot$ (as derived using the NextGen and DUSTY models; Baraffe et al. 1998; Chabrier et al. 2000), can be represented to first order by a slowly rising power law model, $dN/dm \propto m^{-\alpha}$. For example, from their CFHT survey conducted at R_{CFHT} and I_{CFHT} and covering 2.5 square degrees, Bouvier et al. (1998) identified 17 candidate BDs ($I_C \geq 17.8$) and derived a power law index of $\alpha = 0.6 \pm 0.1$. From their 1.1 square degree

INT survey conducted at I_{RGO} and Z_{RGO} , with follow-up work undertaken in the K -band, Dobbie et al. (2002) unearthed 16 candidate substellar members and found a power law index of $\alpha = 0.8 \pm 0.2$ to be consistent with their data. Moraux et al. (2003) extended the CFHT survey to an area of 6.4 square degrees (at I_{CFHT} and Z_{CFHT}) and unearthed a total of 40 candidate BDs. They applied statistical arguments to account for non-members in their sample and derived a power law index of $\alpha = 0.6 \pm 0.1$.

In arguably the most comprehensive deep study of the Pleiades to date, in terms of the selection criteria, Jameson et al. (2002) assembled a sample of candidate substellar cluster members from four relatively recent CCD surveys, the International Time Project survey (Zapatero Osorio et al. 1999), the CFHT survey (Bouvier et al. 1998; Moraux et al. 2001), the Burrell Schmidt survey (Pinfield et al. 2000) and the INT survey (Dobbie et al. 2002). As candidates were selected at the very least on the basis of photometry in three passbands, contamination in the final sample of 49 likely BD members was estimated to be relatively low ($\sim 10\%$). This sample was used to derive an IMF power law index of $\alpha = 0.41 \pm 0.08$ over the $m = 0.3\text{--}0.035 M_\odot$ (Jameson et al. 2002). Moreover, Pinfield et al. (2003) used these objects to infer a low-mass stellar/substellar binary fraction of $50 \pm 10\%$ in the Pleiades. This estimate is at least twice as large as determinations based on high-resolution imaging studies of both old field ultracool dwarfs (10–20%; e.g. Burgasser et al. 2003; Close et al. 2003; Bouy et al. 2003) and Pleiades BDs ($13.3_{-4}^{+13}\%$ Martín et al. 2000, 2003; Bouy et al. 2006a). Additionally, a number of the most detailed current theoretical models of brown dwarf formation predict a substellar binary fraction of only $\sim 5\%$ due to the disruptive influence of dynamical interactions during the earliest stages of their formation (Bate et al. 2002; Delgado-Donate et al. 2003).

However, more recently, Maxted & Jeffries (2005) have conducted Monte-Carlo simulations to reproduce the binary properties of low-mass stars and BDs extracted from a number of radial velocity surveys (Guenther & Wuchterl 2003; Kenyon et al. 2005; Joergens 2006) and have argued that the overall binary frequency is more likely to be in the range 32–45%, comparable to that of K/M dwarfs. Furthermore, Basri & Reiners (2006) have concluded that spectroscopic binaries (i.e. close systems) can account for $\sim 11\%$ over the 0–6 au separation range and should be added to those resolved in the course of high-resolution imaging despite some overlap in the separation ranges probed by both samples. This conclusion was also reached by Maxted & Jeffries (2005), implying that current binary estimates might actually be about twice larger. Nevertheless, the orbital separation and mass ratio distributions of low-mass binaries do appear to differ from those of their higher-mass G–M counterparts (Duquennoy & Mayor 1991; Fischer & Marcy 1992): the low mass separation distribution peaks around 4–8 au and three-quarter of systems have mass ratio larger than $q = 0.8$ (Burgasser et al. 2007).

In this paper we present the results of our analyse of about 12 square degree survey of the Pleiades in $ZYJHK^1$ and released as part of the UKIDSS Galactic Cluster Survey Data Release 1 (DR1) on 21 July 2006 (Warren et al. 2007). In Section 2 we present the multi-epoch observations considered in this study to extract photometric and PM candidate members of the Pleiades, including 2MASS (Cutri et al. 2003), INT (Dobbie et al. 2002; Jameson et al.

¹ $ZYJHK$ are WFCAM filters. Filters from other studies are labelled in the text with the name of the observatory/survey to avoid confusion. However, WFCAM filters are labelled as such in the figures.

2002), CFHT (Moraux et al. 2003), and the UKIDSS GCS (second epoch) surveys. In Section 3 we describe the photometric selection of candidate cluster members from various colour-magnitude diagrams (CMDs) and estimate proper motions (PMs) from a probabilistic analysis. In Section 4 we review the list of previously published members recovered by our survey. In Section 5 we discuss the photometric binary frequency in the substellar regime and compare it with previous estimates in the Pleiades and for ultracool field dwarfs. In Section 6 we derive the cluster luminosity and mass function and discuss the observed features over the mass range probed by the GCS. Finally, we summarise our work in Section 7.

2 SURVEYS AND DATASETS

2.1 The UKIDSS GCS in the Pleiades

The UKIRT Infrared Deep Sky Survey (Lawrence et al. 2006)² is a deep large-scale infrared surveys conducted with the UKIRT Wide-Field CAMera (WFCAM) on Mauna Kea in Hawai'i. The survey is composed of 5 independent components: the Large Area Survey, the Galactic Cluster Survey (hereafter GCS), the Galactic Plane Survey, the Deep Extragalactic Survey, and the Ultra-Deep Survey. All observations are pipeline-processed at the Cambridge Astronomical Survey Unit (CASU; Irwin et al. 2007, in preparation)³. The processed data are then archived in Edinburgh and released to the user community through the WFCAM Science Archive (WSA; Hambly et al. 2007, in preparation)⁴. More details on the specificities of DR1 are given in Warren et al. (2007).

The WFCAM focal plane array consists of 4 Rockwell 2048 × 2048 chips each covering a 13 arcmin by 13 arcmin field (or pawprint) with a pixel scale of 0.4 arcsec. Each detector is separated by about 10 and 10 arcmin in the x and y axes, respectively. Consequently, four pawprints are required to obtain a contiguous coverage (or tile) of 0.8 square degrees (Casali et al. 2007, in preparation). The *Z* and *Y* filters are centred at 0.92 and 1.03 μm, respectively, and are 0.1 μm wide. The *J*, *H*, and *K* near-infrared broad-band filters are in the Mauna Kea Observatory (MKO) system (Hewett et al. 2006).

The GCS will cover ∼1000 square degrees in 10 star-forming regions and open clusters down to *K* = 18.4 mag at two epochs. The main scientific driver of the GCS is to study the IMF and its dependence with environment in the substellar regime using an homogeneous set of observations of low-mass stars and BDs over a large area in several regions. The UKIDSS DR1 contains 50 square degrees in the Pleiades, Hyades, Taurus, and Orion (Warren et al. 2007). The total area released in the Pleiades in *ZYJHK* is approximately 12 square degrees close to the central region of the cluster (Figure 1). The 100% completeness limits of the Pleiades GCS survey are *Z* ≈ 20.1, *Y* ≈ 19.8, *J* ≈ 18.9, *H* ≈ 18.4, and *K* ≈ 17.8 mag.

We have selected point sources in the Pleiades (UKIDSS GCS project #2) in a similar manner as described in our work conducted in Upper Sco (see SQL query in Appendix A of Lodieu et al. 2007). The main upgrades to the selection procedure applied in Upper Sco

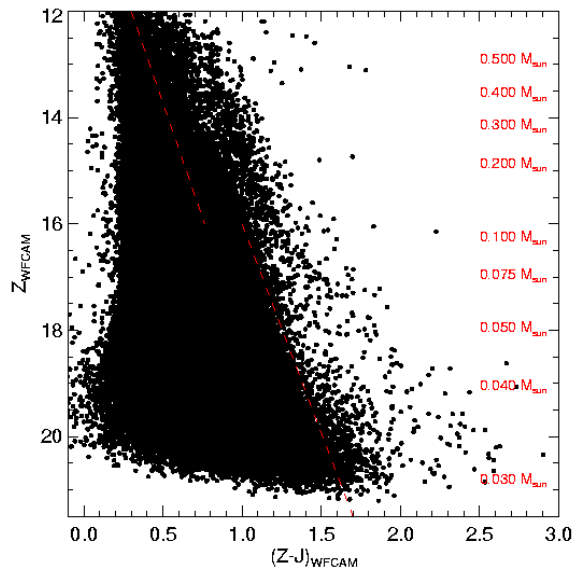


Figure 2. $(Z - J, Z)$ CMD for a 12 square degree area in the Pleiades cluster extracted from the UKIDSS Galactic Cluster Survey Data Release 1. The mass scale is shown on the right hand side of the diagrams and extends down to $0.03 M_{\odot}$, according to the NextGen and DUSTY models (Baraffe et al. 1998; Chabrier et al. 2000). The photometric selection criteria applied to select new candidates in the cluster prior to the derivation of proper motions is shown as a red dashed line.

are two-fold. Firstly, we insisted on detections classified as point sources (CLASS parameters equal to -2 or -1) in all bands and lifted the constraint on *Z* and *Y* by requesting detections in the *JHK* passbands only. Secondly, we have included a more relaxed constraint on the morphological shape of the point sources in all passbands to increase the completeness at the faint end of the survey i.e. we imposed that the CLASSSTAT parameters lie between -3.0 and $+3.0$ in all passbands unless undetected in the *Z* and *Y* filters. The bright saturation limits are found to be *Z* ≈ 11.3, *Y* ≈ 11.5, *J* ≈ 11.0, *H* ≈ 11.3, and *K* ≈ 9.9 mag from the visual inspection of the histogram of the number of stars as a function of magnitude. However, we have only considered sources fainter than *Z* = 12 mag throughout this analysis to avoid saturated objects. As for Upper Sco, the SQL query includes the cross-correlation with 2MASS to compute PMs for all sources with a 2MASS counterpart (the objects undetected in 2MASS are included in the catalogue but PM is not available). The query returned a total of 105,092 sources. The full coverage is displayed in Fig. 1 and the resulting $(Z - J, Z)$ CMD is shown in Fig. 2. Note that the theoretical isochrones plotted in this paper were specifically computed for the WFCAM set of filters and kindly provided by Isabelle Baraffe and France Allard.

2.2 The 2MASS survey in the Pleiades

As mentioned in the previous section, the SQL query includes a cross-correlation of GCS sources with the nearest 2MASS counterpart when available. The typical accuracy of the resulting proper motion measurement is less than 12 mas/yr down to the 2MASS 5σ completeness limit of $J_{2MASS} = 15.8$ mag for the 5–7 year baseline. The coverage considered here overlaps with the study by Adams et al. (2001) which covered the entire cluster up to 10 de-

² The survey is described at www.ukidss.org

³ The CASU WFCAM-dedicated webpage can be found at <http://apm15.ast.cam.ac.uk/wfcam>

⁴ The WFCAM Science Archive is accessible at the URL <http://surveys.roe.ac.uk/wsa>

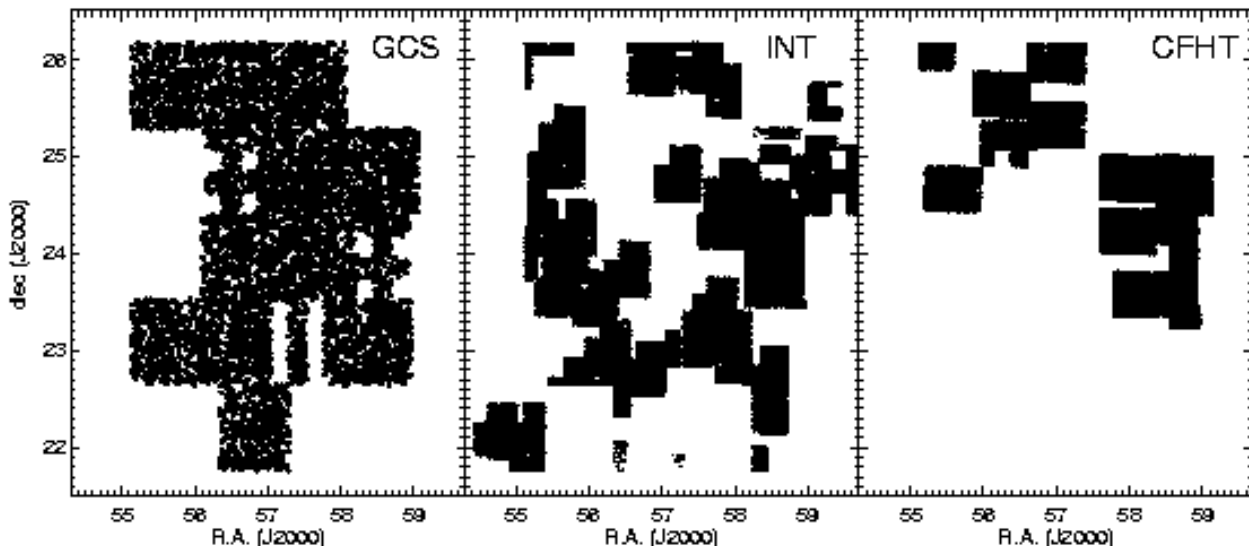


Figure 1. From left to right, coverage used in the Pleiades open cluster to derive PMs: coverage in $ZYJHK$ from the UKIDSS GCS DR1, INT optical survey (e.g. Dobbie et al. 2002), and CFHT I_{CFHT} and Z_{CFHT} study (Moraux et al. 2003). Only one in ten sources are plotted for the GCS coverage. The uneven coverage of the GCS and INT survey is due to the rejection of some tiles after quality control inspection.

Table 1. Main characteristics of the surveys (GCS, 2MASS, CFHT, and INT) used in this study to derive proper motions in the Pleiades cluster. We list the photometric passbands, the completeness limit, the external astrometric accuracy (in arcsec), epoch of observations, and coverage (in square degrees) for each survey. Note that for the CFHT survey, the 90% completeness limit is quoted.

Survey	Filters	Limit mag	Astrom. arcsec	Epoch year	Cov. deg ²
GCS	$ZYJHK$	$J \sim 18.6$	0.1	2005–2006	12
2MASS	JHK_s	$J \sim 15.8$	0.1	1998–2000	300
CFHT	I_{CFHT}	$Z \sim 22.0$	0.2	Dec 2000	6.4
INT	Z_{RGO}	$Z \sim 18.5$	0.3	1998–2000	20

degrees away from the centre and was complete down to $0.1 M_{\odot}$ (Table 1). The level of contamination of this earlier study was estimated to be less than 13% down to $K_{2MASS} = 14$ mag based on an extensive spectroscopic follow-up program of several hundreds of photometric and PM candidates drawn from a cross-correlation between 2MASS (Cutri et al. 2003) and the POSS I and POSS II plates (Reid et al. 1991). However, as a result of less accurate PMs at fainter magnitudes ($K_{2MASS} = 14$ – 14.3 mag), contamination by field stars was at a much higher level, rendering membership assessment at the bottom of this survey considerably less reliable.

2.3 The INT-PL-IZ survey

Approximately 20 square degrees of the Pleiades was surveyed with the INT and Wide Field Camera (WFC) over the course of several semesters between 1998–2000. The WFC consists of four 2048x4196 pixel EEV CCDs with each pixel corresponding to 0.33 arcsec on the sky. Data were obtained using the Z_{RGO} filter and exposure times ranging from 600–1200 seconds in typical seeing of 1.0–1.5 arcsec. The data were reduced at the Cambridge Astro-

nomical Survey Unit using the WFC data reduction pipeline, details of which are given in Irwin & Lewis (2001). Morphological classification and aperture photometry was performed on all sources detected at a significance level of 7σ or greater. Coordinates are accurate to 0.3 arcsec externally (Table 1). Plots of $\log_{10}[\text{number of sources}]$ against magnitude indicate that the vast majority of the Z_{RGO} -band images are photometrically complete to $Z_{RGO} \leq 18.5$ mag, with some data complete to 1.5 magnitudes deeper (e.g. Dobbie et al. 2002) because about half of the INT images were taken under non-photometric conditions. The overlap of the INT data with the GCS survey is depicted in the middle panel of Fig. 1.

2.4 The CFHT survey

The raw CFHT12K data were extracted from the Canadian Astrophysical Data Center archive and were processed at Cambridge University using the same general purpose pipeline described in the previous section (Irwin & Lewis 2001). Characteristics of the re-processed data are given in Table 1 and the coverage falling in the area covered by the GCS is shown in the right panel of Fig. 1. The CFHT survey (and the INT) were used, in this paper, to derive proper motions and not for photometric purposes.

3 NEW SUBSTELLAR MEMBERS IN THE PLEIADES

3.1 An outline of our selection method

In this section we outline our method of selecting very-low-mass stellar and substellar candidate members of the Pleiades using five passband photometry and PMs. The main steps of the procedure are as follows:

- (i) Make a conservative cut in the $(Z - J, Z)$ CMD to select bright ($Z \leq 16$ mag) and faint ($Z \geq 16$ mag) photometric candidates (dashed lines in Fig. 2).

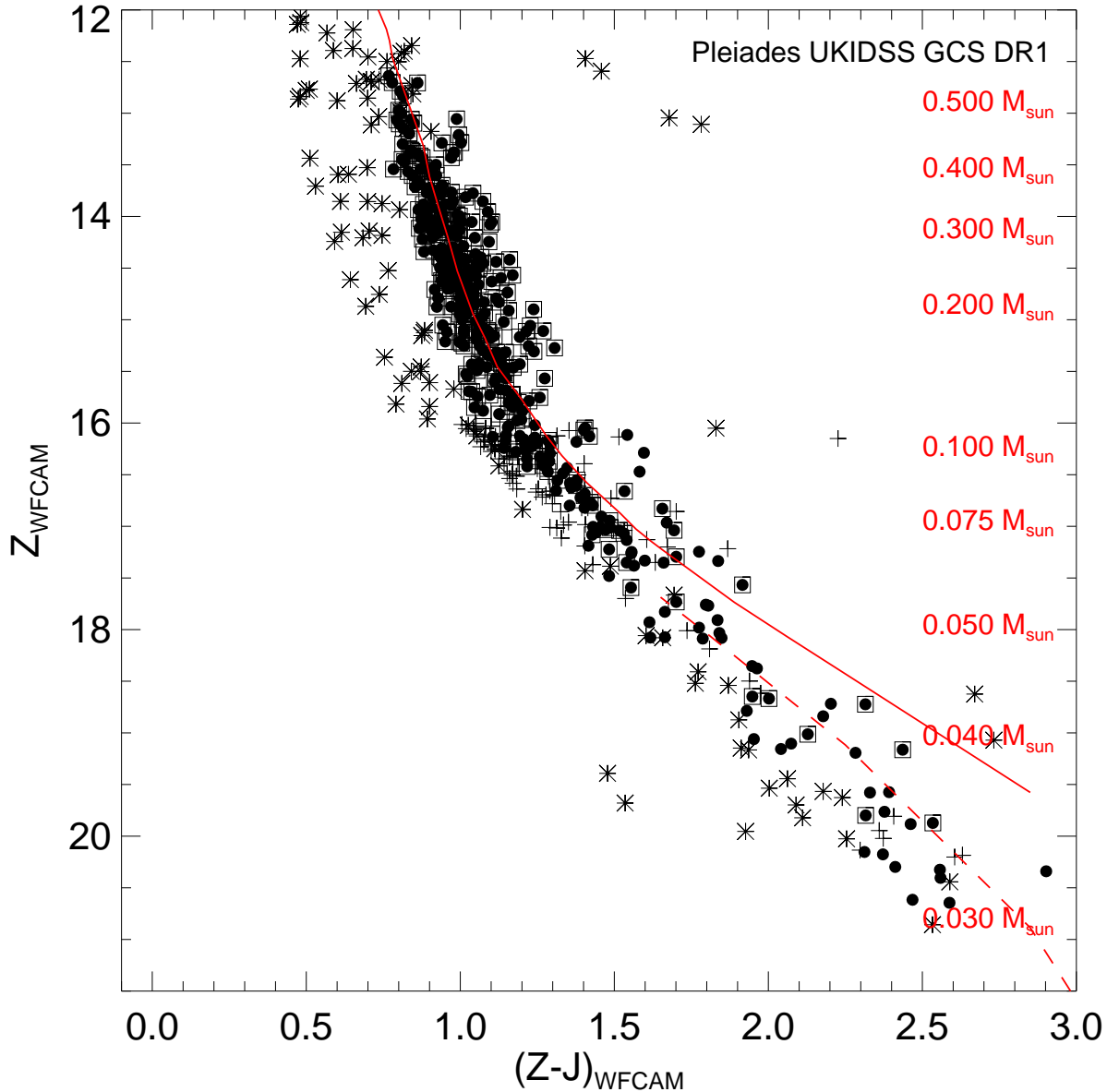


Figure 3. $(Z - J, Z)$ colour-magnitude diagram for all high-probability PM members in the Pleiades (filled dots with open squares) from the cross-correlation of the GCS DR1 with the 2MASS, INT, and CFHT surveys of the clusters. New photometric candidates are shown as filled dots whereas photometric and PM non-members are displayed as star symbols and crosses, respectively. Overplotted are the 120 Myr NextGen (solid line; Baraffe et al. 1998) and DUSTY (dashed line; Chabrier et al. 2000) isochrones. The mass scale is shown on the right hand side of the diagrams and spans 0.5–0.03 M_{\odot} , according to the NextGen and DUSTY 120 Myr isochrones at the distance of the Pleiades.

(ii) Obtain PM from the 2MASS vs GCS cross-correlation for sources brighter than the 2MASS completeness at $Z \sim 17$ mag and from the (INT+CFHT) vs GCS cross-correlation for objects fainter than $Z = 16$ mag (Section 3.2).

(iii) Analyse the vector point diagram in a probabilistic manner and infer a membership probability for each photometric candidate selected in the $(Z - J, Z)$ CMD for which a proper motion measurement exists (Section 3.3). Derive a list of probable cluster members

by choosing a specific threshold for the membership probability ($p \geq 0.6$)

(iv) Weed out any remaining proper motion candidates that have colours in the $(Y - J, Y)$ and $(J - K, J)$ CMDs which are inconsistent with cluster membership (Section 3.3; Table A1).

(v) Select new photometric candidates in the $(Z - J, Z)$ CMD for which no PM is available. Their membership will be constrained further by examining their location in other CMDs and comparing it to proper motion members (Section 3.4)

(vi) Identify new low-mass BD candidates from the $(Y - J, Y)$ CMD i.e. sources undetected in the Z -band

(vii) Identify new possible low-mass BDs from the $(J - K, J)$ CMD i.e. sources undetected in the Z and Y passbands

3.2 Computation of proper motions

3.2.1 2MASS vs GCS cross-correlation

As described in Section 2.2, the SQL query used to retrieve the full Pleiades catalogue from the WSA includes a cross-correlation between the GCS and 2MASS source coordinates to derive PMs. Consequently, PMs are available for all sources brighter than the 2MASS 5σ completeness limit ($J_{2\text{MASS}} = 15.8$ mag; $Z \sim 17.5$ mag) with an accuracy better than 12 mas/yr. The vector point diagram of sources brighter than $Z = 16$ mag and located to the right of a line running from $(Z - J, Z) = (0.3, 12.0)$ to $(1.4, 21.5)$ is shown in the left panel of Fig. 4. The location of the Pleiades cluster stands out clearly in this diagram due to its large PM ($\mu_\alpha \cos\delta \sim 20$; $\mu_\delta \sim -40$ mas/yr). All sources in this diagram are associated with a membership probability and this sample is referred throughout the remainder of this paper as the “bright” sample.

3.2.2 INT and CFHT vs GCS cross-correlation

The completeness of the 2MASS survey is insufficient to derive PMs over the full magnitude range probed by the GCS. However, the Pleiades has been extensively surveyed in the optical over wide area and deeply. Thus, we have cross-correlated the INT and CFHT catalogues (described in Sections 2.3 and 2.4) with the GCS to infer PMs for sources fainter than $Z = 16$ mag (hereafter “faint” sample). Previous optical surveys have achieved similar depths to the GCS, allowing the derivation of PMs down to $Z \sim 21$ mag, corresponding to masses of $30 M_{\text{Jup}}$ for cluster members according to theoretical isochrones (Chabrier et al. 2000). We have adopted on purpose an overlapping range between the “bright” and “faint” samples to scale both luminosity functions (see Section 6). The vector point diagram of GCS sources with optical counterparts is displayed in the right panel of Fig. 4.

The photometric catalogues of the GCS and the CFHT and the GCS and the INT surveys were cross correlated using a matching radius of $2''$. To determine proper motions we constructed 12 coefficient transforms between the coordinates of all sources common to both epochs using routines in the SLALIB package. To minimise the effects of large scale astrometric distortions in the transforms this process was undertaken on a chip by chip basis. Despite the greater depth of the CFHT data relative to the INT data, the resulting proper motion uncertainties are very similar, irrespective of epoch 1 dataset. These are typically found to be 7 mas/yr at $Z = 15$ –18 mag but grow to 12 mas/yr at $Z = 19$ –20 mag.

The $(Z - J, Z)$ CMD is shown in Fig. 3 whereas the corresponding vector point diagram is displayed in Fig. 4.

3.3 Membership probabilities

In order to calculate formal membership probabilities we have used the same technique as Deacon & Hambly (2004) to fit distribution functions to proper motion vector point diagrams (Hambly et al. 1995). First we have rotated the vector point diagram so the cluster lies on the y -axis using the rotation transformation below (Equations 1 and 2):

$$\mu_{x1} = 0.3896 \times \mu_x - 0.921 \times \mu_y \quad (1)$$

$$\mu_{y1} = 0.3896 \times \mu_y - 0.921 \times \mu_x \quad (2)$$

corresponding a rotation angle of 23.7 degrees, assuming a PM of $(19.7, -44.82)$ mas/yr for the Pleiades.

We have assumed that there are two contributions to the total distribution $\phi(\mu_x, \mu_y)$, one from the cluster ($\phi_c(\mu_x, \mu_y)$) and one from the field stars ($\phi_f(\mu_x, \mu_y)$). The fitting region was delineated by $-50 < \mu_x < 50$ mas/yr and $20 < \mu_y < 70$ mas/yr. These were added by means of a field star fraction f to yield an expression for ϕ given in Equation 3:

$$\phi(\mu_x, \mu_y) = f\phi_f(\mu_x, \mu_y) + (1 - f)\phi_c(\mu_x, \mu_y) \quad (3)$$

We have assumed that the cluster distribution is characterised by a two variable gaussian with a single standard deviation σ and mean proper motion values in each axis μ_{xc} and μ_{yc} (Equation 4):

$$\phi_c \propto \exp\left(-\frac{(\mu_x - \mu_{xc})^2 + (\mu_y - \mu_{yc})^2}{2\sigma^2}\right) \quad (4)$$

The field star distribution was fitted by a single gaussian in the x axis (with standard deviation Σ_x and mean μ_{xf}) and a declining exponential in the y axis with a scale length τ (Equation 5). The use of a declining exponential is a standard method (e.g. Jones & Stauffer 1991) and is justified in that the field star distribution is not simply a circularly-symmetric error distribution (i.e. capable of being modelled as a 2d Gaussian) - rather there is a preferred direction of real field star motions resulting in a characteristic velocity ellipsoidal signature, i.e. a non-Gaussian tail, in the vector point diagram. This is best modelled (away from the central error-dominated distribution) as an exponential in the direction of the antapex (of the solar motion).

$$\phi_f \propto \exp\left(-\frac{(\mu_x - \mu_{xf})^2}{2\Sigma_x^2} - \frac{\mu_y}{\tau}\right) \quad (5)$$

Then, we have solved those equations for these seven parameters ($f, \sigma, \mu_{xc}, \mu_{yc}, \Sigma_x, \mu_{xf}, \tau$). This fitting process was tested by Deacon & Hambly (2004) where simulated data sets were created and run through the fitting process to recover the input parameters. These tests produced no significant offsets in the parameter values (see Table 3 and Appendix A of Deacon & Hambly 2004, for results and more details on the procedure). Hence, we have calculated the formal membership probabilities as,

$$p = \frac{\phi_c}{f\phi_f + (1 - f)\phi_c} \quad (6)$$

As the astrometric errors varied in magnitude we have split the sample into six bands. The first three bands (from $Z = 12.0$ to $Z = 18.0$) were each two magnitudes wide and were fitted with all seven parameters in the same way as described in Deacon & Hambly (2004). As the astrometric errors increased rapidly at the faint end, ranges only one magnitude wide were used. In these bands the number of cluster stars was so small so that we have fixed the location of the cluster on the vector point diagram (μ_{xc} and μ_{yc}) to the values from a brighter bin. The other parameters were fitted as normal. A summary of the fitted parameters from the probabilistic analysis described above is given in Table 2.

This sample of 1061 sources with membership probabilities (hereafter “PM sample”) is used to derive the luminosity and mass function in Section 6. Among them, 379 have probabilities equal or higher than 0.6 (or 60%; named hereafter as “high probability PM members”), including 75 that we have classified as photometric non-member after examining their position in several CMDs. The

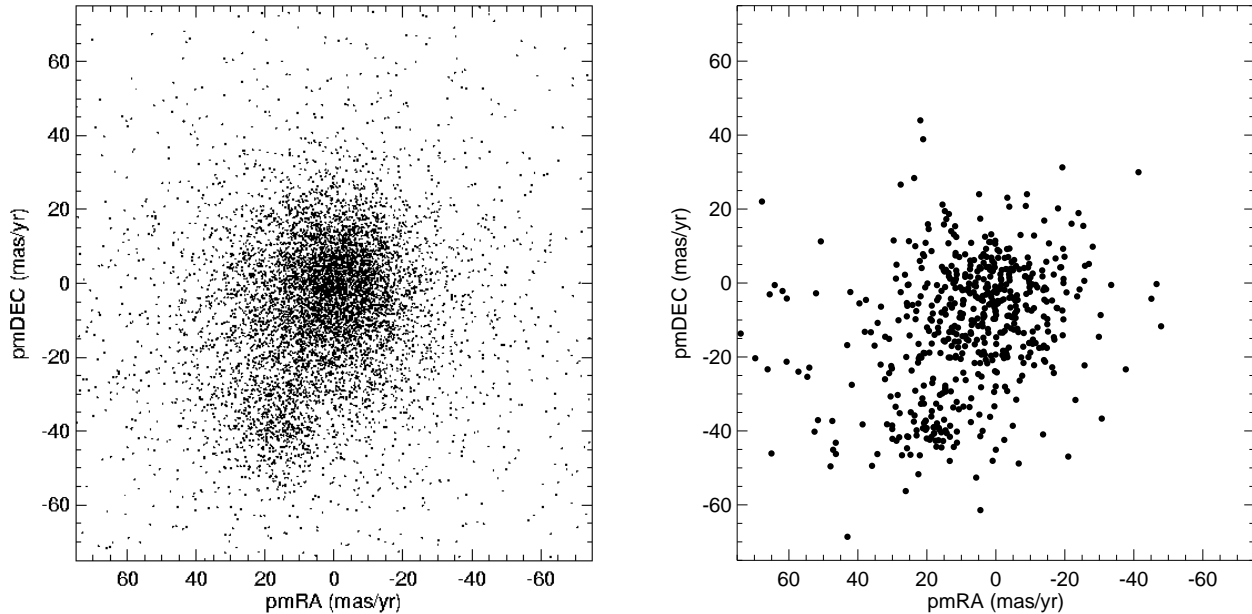


Figure 4. Vector point diagrams (PM in right ascension versus PM in declination) for candidates selected to the right of the dashed lines plotted in Fig. 2: left panel shows bright candidates ($Z \leq 16$ mag) with 2MASS counterparts and the right panel displays fainter sources with INT and CFHT counterparts. The location of the Pleiades cluster is clearly seen around $+20$ and -40 mas/yr in right ascension and declination, respectively.

Table 2. Summary of the results after running the programme to derive membership probabilities. For each Z magnitude range, we list the number of stars used in the fit (Nb), the field star fraction f , and parameters describing the cluster and field star distribution. Units are in mas/yr except for the number of stars and the field star fraction f . The cluster star distribution is described by the mean proper motions in the x and y directions (μ_{x_c} and μ_{y_c}) and a standard deviation σ . Similarly, the field star distribution is characterised by a scale length for the y axis (τ), a standard deviation Σ_x , and a mean proper motion in the x direction (μ_{x_f}).

Z	Nb	f	σ	μ_{x_c}	μ_{y_c}	τ	Σ_x	μ_{x_f}
10–12	12	0.55	7.66	2.38	43.91	6.18	13.58	5.10
12–14	300	0.61	5.95	0.48	40.34	17.79	20.47	2.55
14–16	616	0.63	6.65	0.20	41.71	16.55	17.02	4.21
16–18	82	0.53	4.36	1.81	42.97	22.45	21.96	6.81
18–19	16	0.68	6.53	1.80	42.98	26.15	12.91	7.83
19–20	29	0.68	8.05	1.80	42.98	14.76	11.45	12.07
> 20	18	0.86	10.63	1.80	42.98	11.10	13.61	0.38

mean probability for high probability members is 0.775. In Table A1, we list all high probability PM members fainter than $Z = 16$ mag i.e. masses below $0.1 M_{\odot}$ according to the NextGen models (Baraffe et al. 1998).

3.4 New photometric candidates

The GCS provides a larger areal coverage than the CFHT and INT surveys combined (Fig. 1). As a consequence, there are additional candidates lying on the sequence defined by high probability members ($p \geq 0.6$) in the $(Z - J, Z)$ CMD (Fig. 3) for which no proper motion is available because of a lack of optical coverage. In this section we investigate their membership using the five $ZYJHK$ photometric bands available from the GCS. Those objects are de-

finned thereafter as new photometric candidates and are included in the computation of the binary frequency but not in the derivation of the luminosity and mass functions.

We have considered a straight line passing below the sequence defined by high probability members in the $(Z - J, Z)$ CMD (Fig. 3) and shifted it downwards by 0.2 mag to take into account photometric errors and the depth of the cluster. This line goes from $(Z - J, Z) = (1.0, 16.0)$ to $(2.55, 21.50)$ and the selection returned 230 candidates. Among them are the 46 high probability members (including three classified as photometric non-members; Table A1) as well as 34 low probability objects ($p < 60\%$), yielding a total of $230 - 46 - 34 = 150$ new photometric candidates fainter than $Z = 16$ mag. The first step consisted in cross-correlating them with the list of 2MASS sources brighter than $J = 15.8$ mag to evaluate their membership. Indeed, we have extracted 100 sources in 2MASS, including 53 with PM inconsistent with the Pleiades (outside a circle of radius 25 mas/yr centered on the cluster mean motion; Table B1), leaving 47 PM and 50 photometric candidates for further investigation. The radius of 25 mas/yr corresponds to a detection greater than 3σ for the bright sources and 2σ for the faintest ones, assuming uncertainties on the proper motions derived from the cross-correlation between the GCS and previous optical surveys (Sect. 3.2.2). Inspection of the location of these new candidates in several CMDs, including $(Y - J, Y)$ and $(J - K, J)$, have revealed 24 of them as photometric non-members (Table C1). The rejection is based on the blue colors observed in several diagrams compared to the sequence of PM and photometric members drawn in Sect. 3.3. Consequently, we have 73 new photometric candidates (Table A1) to be added to the high probability PM members.

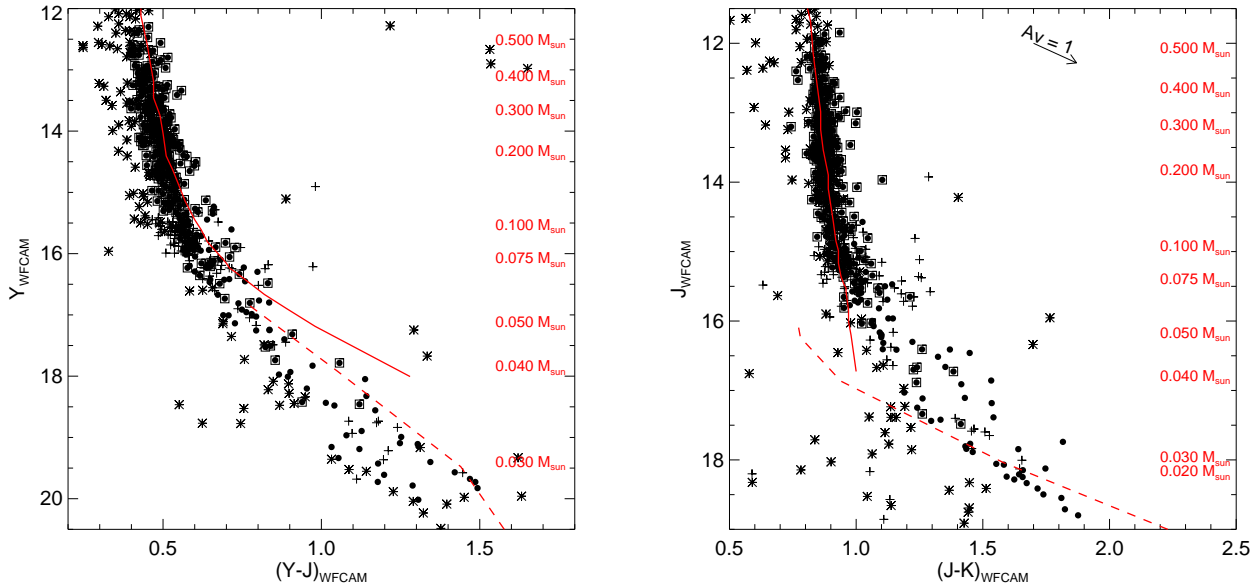


Figure 5. Colour-magnitude diagrams used to extract new low-mass Pleiades BD candidates: *left:* $(Y - J, Y)$ and *right:* $(J - K, J)$. All high-probability PM members are shown as filled dots with open squares. Other symbols are as follows: filled dots are new photometric candidates, star symbols are photometric non-members, and crosses are PM non-members. Overplotted are the 120 Myr NextGen (solid line; Baraffe et al. 1998) and DUSTY (dashed line; Chabrier et al. 2000) isochrones. The mass scale is shown on the right hand side of the diagrams and spans 0.5–0.03 M_{\odot} , according to the 120 Myr isochrone models.

3.5 New faint $YJHK$ candidates

In addition, we have searched for fainter BD candidates using the $(Y - J, Y)$ CMD (left panel in Fig. 5; Table D1) by imposing Z non detection. We have applied the following criteria:

- No Z detection
- $Y = 18.5$ – 21.0 mag
- Candidates should lie above the line defined by $(Y - J, Y) = (0.75, 18.50)$ and $(1.5, 21.0)$

This selection has returned 35 additional candidates (Table D1). Inspection of the $YJHK$ -band images has revealed 9 of them as false or dubious detections (cross-talk, discrepant full-width-half-maximum, lack of detection, etc. . .), leaving 26 sources for further investigation. Among them, nine have a proper motion from the cross-correlation between the (INT+CFHT) surveys and the GCS and five are located within a circle of 25 mas/yr radius centered on the Pleiades mean motion. The probabilistic approach was not feasible due to the small number of Z non-detection with PM. All five photometric and PM members have $J - K$ colours consistent with cluster membership. By the same token, we note that two out of four PM non-members were too blue in $J - K$ whereas the other two sit on the cluster locus and would have been considered as photometric candidates if no PM was available.

Among the remaining $26 - 9 = 17$ sources with no PM, seven fit the cluster sequence in the $(J - K, J)$ CMD while the remaining ten have $J - K$ colours bluer than 1.5 mag. The analysis of the seven sources with PM which also fit the cluster sequence in the $(J - K, J)$ CMD showed that two of them were classified as PM non-members, implying that would expect at least two contaminants among the new sample of seven photometric candidates. Unfortunately, we can only use a statistical approach here, hence

their membership should be treated with caution until PM is available for them after the second observations planned by the GCS.

3.6 New faint JHK candidates

Finally, we have attempted to select JHK -only sources from the $(J - K, J)$ CMD to look for even lower-mass BDs (left panel in Fig. 5; Table E1). We have imposed an upper limit of $J = 18.9$ mag, corresponding to the 100% completeness of the GCS. Our aim was to avoid any bias towards red sources as we might reach the L/T transit predicted at $J \simeq 18.2$ mag by the DUSTY models (Chabrier et al. 2000). Hence, we have cross-correlated all GCS sources in the $J = 17.5$ – 18.9 magnitude range with the INT and CFHT catalogues. We have retrieved 16 photometric sources with PM but only one has a PM consistent with the Pleiades. Scrutiny of the finding charts revealed that only three objects were real detections; the remaining 13 being classified as dubious in Table E1.

If a true member and assuming it is a single star, the faintest photometric and PM candidate in the Pleiades extracted from the GCS has $J \simeq 18.8$ mag and a $J - K$ colour of 1.88, corresponding to a mass of $28 M_{\text{Jup}}$ according to the DUSTY models (Chabrier et al. 2000). We estimate its spectral type to be late-L assuming typical near-infrared colours for field L dwarfs (Vrba et al. 2004): the reddest mean $J - K$ colour is reported for a L8 field dwarf. Hence, the GCS is just short of the transition region where dust settles in the atmosphere of BDs.

Finally, we should mention that the DUSTY models (Chabrier et al. 2000) lie on the high side of the Pleiades sequence in the $(Z - J, Z)$ (Fig. 3) and $(Y - J, Y)$ (left panel of Fig. 5) CMDs. This fact is not surprising as the authors stated themselves in their Section 2 that the DUSTY models represent “extreme situations” i.e. the amount of dust could be overestimated if the dust

Table 3. Summary of the numbers of photometric and PM members, photometric candidates only, PM non-members, and photometric members published by earlier studies and recovered in the GCS area. The quoted percentages include PM and photometric members compared to the total number of sources in the GCS area. References are: Festin (1998), Bouvier et al. (1998), Zapatero Osorio et al. (1999, ZO99), Hambly et al. (1999), Pinfield et al. (2000), Deacon & Hambly (2004, DH04), and Bihain et al. (2006).

Survey	Memb	PM_LNM	photNM	cand	All	%
Festin98	14	2	2	4	22	72.7
Bouvier98	15	—	7	1	24	62.5
ZO99	8	4	3	12	24	62.5
Hambly99	4	—	1	—	5	80.0
Pinfield00	160	—	45	—	205	78.0
Morau03	11	—	6	6	20	55.0
DH04	275	—	0	—	275	100.0
Bihain06	20	1	2	1	24	87.5

if not in equilibrium with the gas phase in brown dwarf’s photospheres. We find that if we assume that the DUSTY models match the binary sequence (see Section 5 for the selection of photometric binaries), the errors on the colours and magnitudes could be as high as 0.2 and 0.75 mag, respectively. These errors translate into uncertainties of 200–400 K on the effective temperatures and 0.01–0.02 M_{\odot} in masses, depending on the mass of the object. Furthermore, the DUSTY models cross the cluster sequence in the $(J - K, J)$ CMD (right panel of Fig. 5), suggesting that masses might be underestimated for BDs more massive than $\sim 0.04 M_{\odot}$ and underestimated for lower masses. However, no models can currently reproduce M to L spectral type transition satisfactorily and several groups are working on this issue (France Allard, personal communication).

4 CROSS-CORRELATION WITH PREVIOUS SURVEYS

The selection of cluster candidates described above yielded a large number of previously published Pleiades members reported in the literature (references therein). In particular, all bright members down to $Z = 16$ mag (corresponding to masses of $\sim 0.1 M_{\odot}$) reported in previous survey such as Hambly et al. (1993), Adams et al. (2001), and Deacon & Hambly (2004), were recovered by our study. In Table 3 we summarise the numbers of proper motion members, photometric candidates, proper motion and photometric low-mass stars and BD non-members published by earlier studies (Festin 1998; Bouvier et al. 1998; Zapatero Osorio et al. 1999; Hambly et al. 1999; Pinfield et al. 2000; Deacon & Hambly 2004; Bihain et al. 2006). Note that the list published by Deacon & Hambly (2004) contains only sources with membership probabilities higher than 0.6 and are recovered in the GCS as such.

We provide an electronic table which summarises the information on previous Pleiades candidates published by earlier studies and recovered in the GCS area (Table 4). This table lists the coordinates (J2000), the GCS photometry in 5 passbands ($ZYJHK$), PMs, their membership probabilities, as well as their associated names (including those attributed by previous surveys to the best of our knowledge).

Table 5. Number of photometric multiple system candidates as a function of magnitudes extracted from the $(Y - K, K)$ CMD and confirmed in the $(J - K, K)$ diagram (Table F1). Proper motion members and new photometric candidates are included in the computation of the binary fraction (BF). Columns list the K magnitude range, the mass range derived for single stars assuming an age of 120 Myr, the total number of single stars+systems, the number of single stars, the number of multiple systems (N_{bin}), and the binary fraction. Those calculations suggest a substellar binary frequency of 28–44% over the 0.075–0.040 M_{\odot} mass range.

K range	Mass range	All	Single	N_{bin}	BF
14.5–15.5	0.075–0.045	42	27	15	35.7%
15.0–16.0	0.055–0.040	25	15	10	40.0%
15.5–16.5	0.045–0.030	21	13	8	38.1%
14.5–16.5	0.075–0.030	63	40	23	36.5%

5 DISCUSSION ON THE BINARY FREQUENCY

In this section, we investigate the binary frequency of BDs in the Pleiades using the photometry and colours from the GCS. The multiplicity in the substellar domain constitutes one way to constrain the formation mechanisms of BDs.

The single-star sequence and its associated binary sequence lying 0.75 mag above are clearly visible in the $(Y - K, K)$ CMD (Fig. 6). We have selected substellar multiple system candidates from this diagram (circled dots in Fig. 6) and listed them in Table F1. The multiplicity of those candidates was confirmed in their position in the $(J - K, K)$ diagram (right panel in Fig. 6)⁵. The selection was made as follows: for a given magnitude, say $K = 15.5$ – 16.5 mag, we have drawn two horizontal lines (dashed lines in Fig. 6) intercepting the single object sequence which we have interpolated using high probability PM members available from the optical/infrared cross-correlation (Section 3.2). From the intercept points we have drawn two vertical lines with a length of 0.75 mag. Then we have divided the box formed by both sequences and the vertical lines into two boxes: single stars lie in the bottom part whereas binary candidates in the top one. The dividing line between the lower and upper box was chosen to go through the gap present between the single-star and binary sequences, corresponding to a mass ratio of ~ 0.4 . The binary fraction was then defined as the number of binaries divided by the total number of objects (single stars+binaries).

In total, we have counted 23 substellar multiple system candidates in the $K = 14.5$ – 16.5 mag range (corresponding to masses between 0.075 and 0.030 M_{\odot}) and 40 single objects, yielding a binary frequency of $23/(23+40) = 36.5 \pm 8.0\%$ assuming Poisson errors (Table 5). These candidates include high probability members and new photometric candidates. The binary frequency range across the substellar regime probed by our survey is more likely to lie between 35 and 40% according to the dispersion as a function of mass (Table 5).

Our estimate of the substellar binary frequency is likely to be a lower limit for two reasons. Firstly, high-mass ratio binaries i.e. the ones with very low-mass companions will have hardly moved away from the single star sequence. For example, the crosses plotted in the left panel of Fig. 6 represent a 20, 30, 40, and 50 M_{Jup}

⁵ We note that a few candidates lie in the binary sequence in the $(J - K, K)$ CMD but were not selected in the $(Y - K, K)$ CMD. These sources could be either lower mass ratio systems or reddened cluster members

Table 4. Sample of objects from the electronic table: we list the equatorial coordinates (J2000), GCS *ZYJHK* photometry, proper motions (mas/yr), names from the previous studies in the cluster, and membership (Memb≡photometric and PM member; cand≡photometric candidate, PM_NM≡ PM non-member, photNM≡photometric non-member).

R.A.	Dec.	Z	Y	J	H	K	$\mu_{\alpha} \cos \delta$	μ_{δ}	Name	Memb?
03 54 01.43	23 49 57.6	99.999	99.999	18.704	17.696	16.984	—	—	BRB29	cand
03 54 02.55	24 40 25.9	20.435	19.257	18.369	17.945	17.142	10.19	-20.53	CFHTPLIZ34	photNM
...
03 54 14.06	23 17 52.0	19.946	18.760	17.586	16.789	16.131	26.13	-56.27	CFHTPLIZ28, BRB18	Memb
03 54 38.37	23 38 01.1	20.684	19.314	18.480	17.908	17.366	-5.85	4.61	CFHTPLIZ36	PM_NM

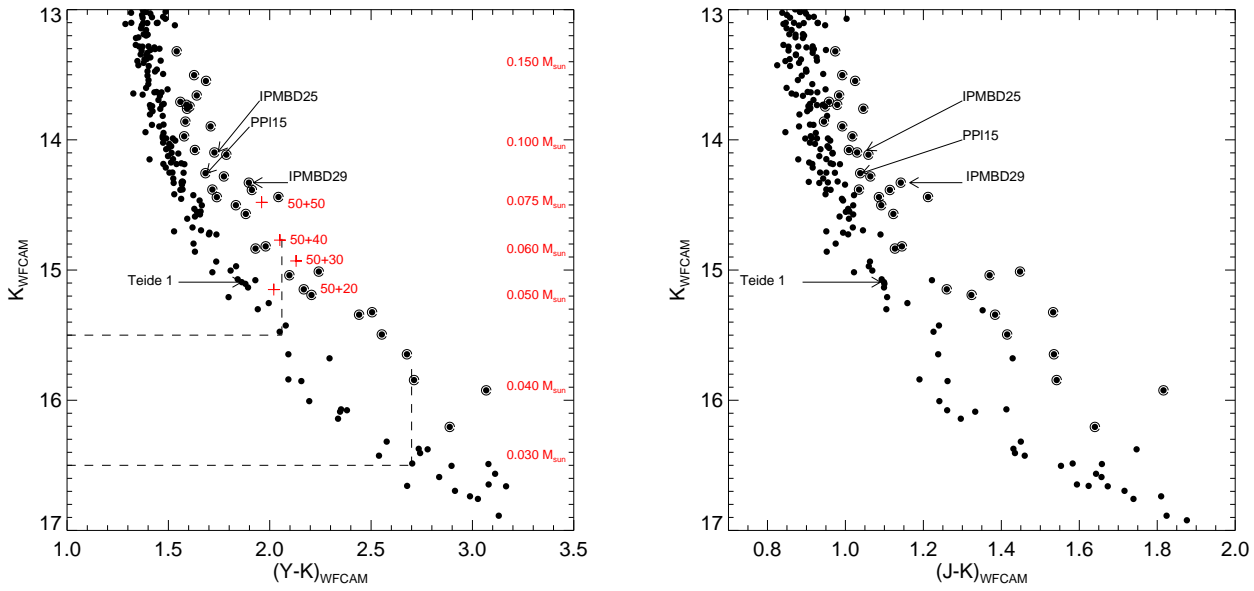


Figure 6. $(Y - K, K)$ and $(J - K, K)$ CMDs for all substellar Pleiades candidates extracted from the UKIDSS GCS. We have originally used the $(Y - K, K)$ diagram to pick out substellar photometric multiple system candidates highlighted with an open circle around filled dots. We have confirmed all of them from their location in the $(J - K, K)$ diagram. We have found a total of 23 photometric multiple systems out of 63 candidates in the substellar regime ($K \geq 14.5$ mag or masses below $0.075 M_{\odot}$), yielding a photometric binary fraction of 33-40%. We have highlighted a number of known binaries in the Pleiades, including PPI 15, a spectroscopic binary brown dwarf with a mass ratio of 0.85 (Basri & Martín 1999), IPMBD 25, and IPMBD 29 (Bouy et al. 2006a) as well as Teide 1 which sits in the single star sequence and for which no companion as been reported to date.

BD added to a $50 M_{\text{Jup}}$ BD, respectively. The computation of the sequence of binaries with successively more massive companions was done using the Lyon group models for K magnitudes and empirical data for Y magnitudes. Adding intensities for various mass combinations and reconvert to magnitudes gave the crosses in Fig. 6. It can be seen that low-mass ratio binary systems will hardly stand out from the single star sequence, hence difficult to pick out in a photometric-based search. As a consequence of the choice of our dividing line, we should be sensitive to mass ratios greater than 0.4 as are high-resolution imaging surveys. Secondly, the single star sequence is more likely to be affected by field dwarfs and reddened background stars than the binary sequence. Additionally, we need to take into account the depth of the cluster. The Pleiades has a tidal radius of 13 pc (Pinfield et al. 2000) and a distance of 130 pc, implying that the distance of any member can vary by $\pm 10\%$ corresponding to a variation of ± 0.2 magnitude.

On average, we have derived a BD binary fraction of 28-44% in the Pleiades cluster, two to three times larger than estimates from high-resolution imaging survey ($13.3_{-4}^{+13}\%$; Martín et al. 2000,

2003; Bouy et al. 2006a). The upper limit from the *HST* surveys in the Pleiades is lower than our estimates. We probe a wider mass range ($75-30 M_{\text{Jup}}$ vs $65-55 M_{\text{Jup}}$) and a comparable mass ratio range ($q \geq 0.5$) than those high-resolution surveys. Furthermore, our estimate is lower than the photometric estimate of $50 \pm 10\%$ by Pinfield et al. (2000) although consistent within the uncertainties. Recently, Basri & Reiners (2006) inferred an upper limit of $26 \pm 10\%$ on the binary fraction of low-mass stars and BDs, divided up into 11% of spectroscopic binaries (0-6 au) and 15% of wider binaries (3-15 au) despite some overlap between both subsample. Our results are on the high side of this latter estimate but compatible considering the uncertainties on both measurements. Finally, our results are in excellent agreement with the frequency of 32-45% from Monte-Carlo simulations (Maxted & Jeffries 2005). Our results are not reproduced by current theoretical models predicting a low fraction of substellar binaries (Bate et al. 2002; Delgado-Donate et al. 2003) and represent a challenge for current theory of brown dwarf formation. Moreover we find a gap between the single and binary sequences, suggesting that most BDs tend

to harbour equal-mass ratios seven sources have $q=0.6-0.8$; 15 have $q=0.8-1.0$; two have $q<0.6$, and twelve are undetermined), similar to the properties of field BDs (mass ratios are listed in the last column of Table 5). Furthermore, we have recovered two known binaries resolved by *HST* (IPMBD 25 and 29) and one object observed by *HST* but not resolved (CFHT-P1-IZ 4) as well as PPI15, suggesting that high-resolution surveys could be missing half of the binaries, hypothesis consistent with the conclusions drawn by Basri & Reiners (2006). Finally, the binary fraction could be dependent on the environment with a possible higher frequency in clusters than the field (Pinfield et al. 2000; Maxted & Jeffries 2005; Kraus et al. 2006; Bouy et al. 2006b; Burgasser et al. 2007), trend reproduced by a model proposed by Goodwin & Whitworth (2007). However, there is currently no direct evidence for such a dependence mainly due to the lack of statistics and the uncertainties on membership in young clusters (Kraus et al. 2006; Bouy et al. 2006b).

6 THE INITIAL MASS FUNCTION

In this section we discuss the cluster luminosity and mass function derived from the sample of candidates with PM from the “bright” (2MASS) and “faint” (INT+CFHT) samples. We do not consider here the new photometric candidates (Section 3.4) because of a lack of PMs and did not attempt to correct the mass function for binaries.

6.1 The cluster luminosity function

In this section, we consider all photometric candidates with membership probabilities i.e. 1061 sources with Z magnitudes ranging from 12 to 21.5 mag (Section 3.4). Assuming that the lithium depletion boundary is at $M \sim 0.075 M_{\odot}$ ($M_Z = 11.44$ Stauffer et al. 1998; Barrado y Navascués et al. 2004) and a distance of 130 pc, our sample contains 967 stars and 94 BDs. Those numbers objects should not be seen as exact numbers as they are subject to a 0.15 mag uncertainty in the position of the lithium depletion boundary but imply that our sample contains $10_{-0.5}^{+1.6}\%$ of substellar objects (the number of BDs varies from 82 to 98). The luminosity function is usually defined as the number of stars as a function of magnitude but here we have derived it in a probabilistic manner: we summed the membership probability of all 1061 sources divided up into 0.5 magnitude bin instead of simply counting the number of objects. We have two independent samples: on the one hand, the “bright” sample considered down to $Z = 16$ mag and the “faint” sample used for fainter candidates. Both samples are complete over the $Z = 16.25-16.75$ magnitude range as demonstrated in the left-hand side panel of Fig. 7.

The “faint” sample was not drawn from the full GCS sample (hence coverage) because of the limited areal optical coverage and, thus, need to be scaled to the “bright” sample. We have investigated two approaches to infer a scaling factor over the $Z = 16.25-16.75$ magnitude range where both samples were complete. The total number of sources with proper motions in this magnitude range is 5988 and 2976 for the bright and faint samples, respectively. Hence, the ratio of the number of sources gives a scaling factor of $5288/2976 = 1.777$. The second consisted in summing the probabilities for the “bright” and “faint” samples in the same magnitude range as above. The inferred scaling factor is $20.217/12.114 = 1.669$. Hence, we have favoured the first method (which is likely less affected by uncertainties) and scaled the luminosity function of the “faint” sample by a factor of 1.777 to match the “bright”

sample. The error on the scaling factor is less than 0.1 since both methods give similar results.

The sum of membership probabilities after scaling and correction for incompleteness are given in Table 6 and plotted in the right-hand side panel of Fig. 7. Error bars are Gehrels errors (Gehrels 1986) rather than Poissonian error bars because the former represent a better approximation to the true error for small numbers. The upper limit is defined as $1+(\sqrt{dN + 0.75})$ and the lower limit as $\sqrt{dN - 0.25}$ assuming a confidence level of one sigma. Incompleteness and scaling factors were applied to the errors when necessary. The luminosity function peaks at $Z \sim 14.5-15.0$ mag and decreases down to $Z \sim 18.0-18.5$ mag where it bounces back down to the survey limit (right-hand side panel of Fig. 7). The last two bins are subject to large incompleteness factors and should be treated with caution. Similarly, the brightest bin is likely to be affected by incompleteness.

6.2 The cluster mass function

In this section we adopt the following definition for the mass function as originally proposed by Salpeter (1955): $\xi(\log_{10} m) = dn/d\log_{10}(m) \propto m^{-\alpha}$. We have converted the luminosity into a mass function using the NextGen models (Baraffe et al. 1998) for stars and BDs more massive than $50 M_{Jup}$ (T_{eff}) and the DUSTY models (Chabrier et al. 2000) below. The $Z = 12-21.5$ magnitude range translates into masses between 0.65 and $0.03 M_{\odot}$, assuming a distance of 130 pc and an age of 120 Myr. This mass range is in agreement with the estimated masses given in Table 2 in Schwartz & Becklin (2005), suggesting that we have detected mid-L dwarfs in the Pleiades. The latter authors used the DUSTY models (Chabrier et al. 2000) and Burrows models (Burrows et al. 1997, 2000) at 80 and 125 Myr to infer a possible mass range for their new BD candidates. The faintest photometric and PM candidate extracted from the $(J - K, J)$ CMD but not included in this mass function exhibit red infrared colours (Section 3.6), implying that we are not probing the L/T transition in the Pleiades where dust settles in the atmosphere of BDs.

The mass function, derived from the sample of sources with membership probabilities, is shown in the left-hand side panel of Fig. 8. This mass function is the “unresolved system” mass function since we did not attempt to correct for binaries (Morau et al. 2004). Similarly we did not correct for the radial distribution of low-mass stars and BDs in the cluster due to the inhomogeneous coverage currently available from the GCS. On inspection of the mass function (Fig. 8) it was decided that a single power law would not properly represent the functional form over the full range of masses. Hence we have considered three mass ranges where we have fitted a power law: $0.563-0.333 M_{\odot}$ (filled circles), $0.333-0.116 M_{\odot}$ (star symbols), and $0.116-0.035 M_{\odot}$ (open squares). Each segment in the mass range is best characterised by power law indices α of 0.98 ± 0.87 , -0.18 ± 0.24 , -2.11 ± 1.20 , respectively. Those results are in agreement within the uncertainties with previous studies of the Pleiades mass function in the low-mass star and brown dwarf regimes (Martín et al. 1998; Dobbie et al. 2002; Tej et al. 2002; Morau et al. 2003; Deacon & Hambly 2004). Adams & Fatuzzo (1996) proposed that the initial mass function can be approximated by a lognormal function defined by:

$$\log_{10} \xi(\log_{10} m) = a_0 + a_1 \times \log_{10} m + a_2 \times (\log_{10} m)^2 \quad (7)$$

The best lognormal function fit to the mass function (dashed line in

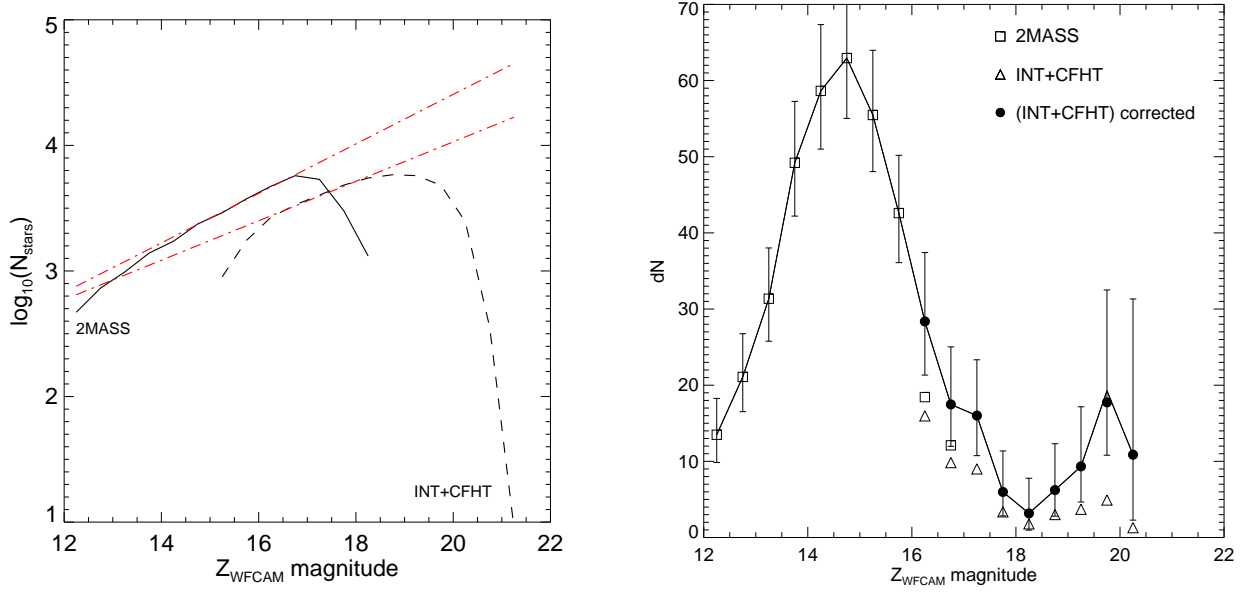


Figure 7. *Left:* The number of stars as a function of magnitude for the “bright” (2MASS; solid line) and “faint” (INT+CFHT; dashed line) samples. The red dot-dashed lines represent the linear fit to both sets of data and are used to estimate their incompleteness. Both samples are complete in the $Z = 16.25$ – 16.75 magnitude range, implying a scaling factor of 1.777. *Right:* The Pleiades luminosity function, defined as the sum of all membership probabilities per 0.5 magnitude bins, for all candidates in the $Z = 12.0$ – 21.5 magnitude range. The “bright” sample is shown as open squares whereas the “faint” sample is depicted as open triangles. The filled circles represent the “faint” sample corrected for incompleteness and scaling. The last two points are not plotted because outside the plot scale. Error bars are Gehrels error bars.

Table 6. Luminosity and mass function for the Pleiades open cluster using the NextGen and DUSTY 120 Myr theoretical isochrones and a distance of 130 pc. The incompleteness factor (InFactor) applied to the faint end of the luminosity function are quoted as well as the scaling factor (ScFactor) of 1.777 applied to the “faint” sample to take into account the limited optical coverage from the INT and CFHT surveys and match the “bright” sample. Gehrels errors, scaled by the incompleteness and scaling factors, are listed for the luminosity and mass functions (errH and errL stand for upper and lower error bars, respectively).

Mag range	Mass range	Mid-mass	dN	errH	errL	InFactor	ScFactor	dN/dM	errH	errL
12.0-12.5	0.6470-0.5630	0.60500	13.5	4.8	3.6	1.00	1.000	160.6	56.8	43.3
12.5-13.0	0.5630-0.4940	0.52850	21.1	5.7	4.6	1.00	1.000	305.7	82.2	66.2
13.0-13.5	0.4940-0.4170	0.45550	31.4	6.7	5.6	1.00	1.000	407.2	86.6	72.4
13.5-14.0	0.4170-0.3330	0.37500	49.2	8.1	7.0	1.00	1.000	585.7	96.0	83.3
14.0-14.5	0.3330-0.2520	0.29250	58.6	8.7	7.6	1.00	1.000	724.0	107.5	94.3
14.5-15.0	0.2520-0.1920	0.22200	63.0	9.0	7.9	1.00	1.000	1049.2	149.7	132.0
15.0-15.5	0.1920-0.1460	0.16900	55.5	8.5	7.4	1.00	1.000	1206.0	184.7	161.6
15.5-16.0	0.1460-0.1160	0.13100	42.6	7.6	6.5	1.00	1.000	1420.0	252.8	216.9
16.0-16.5	0.1160-0.0920	0.10400	28.4	6.4	5.3	1.00	1.777	1182.2	266.5	221.0
16.5-17.0	0.0920-0.0750	0.08350	17.5	5.3	4.2	1.00	1.777	1027.8	309.9	244.1
17.0-17.5	0.0750-0.0645	0.06980	16.0	5.1	4.0	1.00	1.777	1524.5	485.1	378.1
17.5-18.0	0.0645-0.0558	0.06020	6.0	3.6	2.4	1.00	1.777	687.7	413.2	275.2
18.0-18.5	0.0558-0.0495	0.05270	3.2	3.0	1.7	1.00	1.777	504.0	473.2	271.5
18.5-19.0	0.0495-0.0416	0.04560	6.2	3.6	2.4	1.16	1.777	789.0	461.1	309.6
19.0-19.5	0.0416-0.0377	0.03960	9.3	4.2	3.0	1.43	1.777	2394.1	1070.8	772.9
19.5-20.0	0.0377-0.0349	0.03630	19.3	5.5	4.4	2.03	1.777	6881.4	1955.0	1557.5
20.0-20.5	0.0349-0.0321	0.03350	10.9	4.4	3.3	4.74	1.777	3882.9	1574.7	1164.0
20.5-21.0	0.0321-0.0298	0.03095	72.9	9.6	8.5	39.29	1.777	31695.7	4166.1	3705.9
21.0-21.5	0.0298-0.0289	0.02935	268.1	17.4	16.4	1862.86	1.777	297926.7	19330.8	18185.7

the left hand side panel of Fig. 8) is given by the following parameters: $a_0 = 1.99$, $a_1 = -2.37$, and $a_2 = -1.89$ over the 0.56 – $0.035 M_{\odot}$ mass range. These parameters can be converted into those defined by Chabrier (2003) to yield $m_c \sim 0.24$ and $\sigma \sim 0.34$. The value of m_c is in good agreement with the value of 0.22 found by Chabrier (2003) for a mass function which includes unresolved

multiple systems. However the value of σ (0.59) does differ from our results. How significant this difference is is impossible to say as Chabrier did not publish errors on his parameters.

It is clear that mass function deviates from a single power law over the course of our sample, with a peak around $0.24 M_{\odot}$. In order to compare these results with those from previous studies

an α plot was produced showing the variation in the value of α over the full mass range (right hand side panel in Fig. 8). The results from several other studies are plotted here too (Martín et al. 1998; Hambly et al. 1999; Tej et al. 2002; Moraux et al. 2003; Deacon & Hambly 2004). It can be seen that the lognormal functions published by Hambly et al. (1999) and Deacon & Hambly (2004) are also in reasonable agreement with these results.

7 SUMMARY

We have presented a deep wide-field survey conducted in the Pleiades open cluster as part of the UKIDSS Galactic Cluster Survey. We have employed a photometric selection complemented with a PM probabilistic analysis to assess the membership of Pleiades member candidates. We have recovered bright members from previous photometric and PM surveys down to $0.1 M_{\odot}$. Below this limit, we present a catalogue of high probability PM members as well as new photometric BD candidates down to $0.03 M_{\odot}$. The main outcomes of the GCS study in the central region of the Pleiades are two-fold:

- we have derived a BD binary fraction around 33–40% in the 0.075 – $0.030 M_{\odot}$ mass range using the sample of high probability PM members as well as the photometric sample. This estimate is in agreement with Monte-Carlo simulations of Maxted & Jeffries (2005) and on the upper side of the estimate from the radial velocity survey conducted by Basri & Reiners (2006). The inferred binary frequency is however on the low side of the photometric estimate by Pinfield et al. (2003) and significantly higher than predictions by high-resolution imaging surveys. The separations and mass ratios seems however consistent with findings for ultracool field dwarfs and BDs in the Pleiades.

- we have derived the Pleiades luminosity function using the sample of photometric candidates with membership probabilities. We have inferred a mass function in the 0.56 – $0.03 M_{\odot}$ and fitted a lognormal function peaking at $0.24 M_{\odot}$ which in agreement with previous studies in the cluster.

ACKNOWLEDGMENTS

This work is based in part on data obtained as part of the UKIRT Infrared Deep Sky Survey (UKIDSS). Part of this work was carried out in Leicester where NL and PDD were postdoctoral research associates funded by the UK PPARC. We are grateful to Isabelle Baraffe and France Allard for providing us with the NextGen, DUSTY and COND models for the WFCAM filters. We thank our colleagues at the UK Astronomy Technology Centre, the Joint Astronomy Centre in Hawaii, the Cambridge Astronomical Survey and Edinburgh Wide Field Astronomy Units for building and operating WFCAM and its associated data flow system. This research has made use of the Simbad database, operated at the Centre de Données Astronomiques de Strasbourg (CDS), and of NASA's Astrophysics Data System Bibliographic Services (ADS). This publication has also made use of data products from the Two Micron All Sky Survey, which is a joint project of the University of Massachusetts and the Infrared Processing and Analysis Center/California Institute of Technology, funded by the National Aeronautics and Space Administration and the National Science Foundation.

REFERENCES

- Adams F. C., Fatuzzo M., 1996, *ApJ*, 464, 256
 Adams J. D., Stauffer J. R., Monet D. G., Skrutskie M. F., Beichman C. A., 2001, *AJ*, 121, 2053
 Béjar V. J. S., et al. 2001, *ApJ*, 556, 830
 Baraffe I., Chabrier G., Allard F., Hauschildt P. H., 1998, *A&A*, 337, 403
 Baraffe I., Chabrier G., Allard F., Hauschildt P. H., 2002, *A&A*, 382, 563
 Barrado y Navascués D., Stauffer J. R., Jayawardhana R., 2004, *ApJ*, 614, 386
 Basri G., Martín E. L., 1999, *AJ*, 118, 2460
 Basri G., Reiners A., 2006, *AJ*, 132, 663
 Bate M. R., Bonnell I. A., Bromm V., 2002, *MNRAS*, 332, L65
 Bihain G., Rebolo R., Béjar V. J. S., Caballero J. A., Bailer-Jones C. A. L., Mundt R., Acosta-Pulido J. A., Manchado Torres A., 2006, *A&A*, 458, 805
 Bouvier J., Stauffer J. R., Martín E. L., Barrado y Navascués D., Wallace B., Béjar V. J. S., 1998, *A&A*, 336, 490
 Bouy H., Brandner W., Martín E. L., Delfosse X., Allard F., Basri G., 2003, *AJ*, 126, 1526
 Bouy H., Martín E. L., Brandner W., Zapatero-Osorio M. R., Béjar V. J. S., Schirmer M., Huélamo N., Ghez A. M., 2006b, *A&A*, 451, 177
 Bouy H., Moraux E., Bouvier J., Brandner W., Martín E. L., Allard F., Baraffe I., Fernández M., 2006a, *ApJ*, 637, 1056
 Briceño C., Luhman K. L., Hartmann L., Stauffer J. R., Kirkpatrick J. D., 2002, *ApJ*, 580, 317
 Burgasser A. J., Kirkpatrick J. D., Reid I. N., Brown M. E., Miskay C. L., Gizis J. E., 2003, *ApJ*, 586, 512
 Burgasser A. J., Reid I. N., Siegler N., Close L., Allen P., Lowrance P., Gizis J., 2007, in Reipurth B., Jewitt D., Keil K., eds, *Protostars and Planets V Not Alone: Tracing the Origins of Very-Low-Mass Stars and Brown Dwarfs Through Multiplicity Studies*. pp 427–441
 Burrows A., Marley M., Hubbard W. B., Lunine J. I., Guillot T., Saumon D., Freedman R., Sudarsky D., Sharp C., 1997, *ApJ*, 491, 856
 Burrows A., Marley M. S., Sharp C. M., 2000, *ApJ*, 531, 438
 Chabrier G., 2003, *ApJL*, 586, L133
 Chabrier G., Baraffe I., Allard F., Hauschildt P., 2000, *ApJ*, 542, 464
 Close L. M., Siegler N., Freed M., Biller B., 2003, *ApJ*, 587, 407
 Cutri R. M., et al. 2003, *2MASS All Sky Catalog of point sources*, 2246
 Deacon N. R., Hambly N. C., 2004, *A&A*, 416, 125
 Delgado-Donate E. J., Clarke C. J., Bate M. R., 2003, *MNRAS*, 342, 926
 Dobbie P. D., Kenyon F., Jameson R. F., Hodgkin S. T., Pinfield D. J., Osborne S. L., 2002, *MNRAS*, 335, 687
 Dobbie P. D., Pinfield D. J., Jameson R. F., Hodgkin S. T., 2002, *MNRAS*, 335, L79
 Duquennoy A., Mayor M., 1991, *A&A*, 248, 485
 Festin L., 1998, *A&A*, 333, 497
 Fischer D. A., Marcy G. W., 1992, *ApJ*, 396, 178
 Gatewood G., de Jonge J. K., Han I., 2000, *ApJ*, 533, 938
 Gehrels N., 1986, *ApJ*, 303, 336
 Goodwin S. P., Whitworth A., 2007, *A&A*, 466, 943
 Guenther E. W., Wuchterl G., 2003, *A&A*, 401, 677
 Hambly N. C., Hawkins M. R. S., Jameson R. F., 1993, *A&AS*, 100, 607

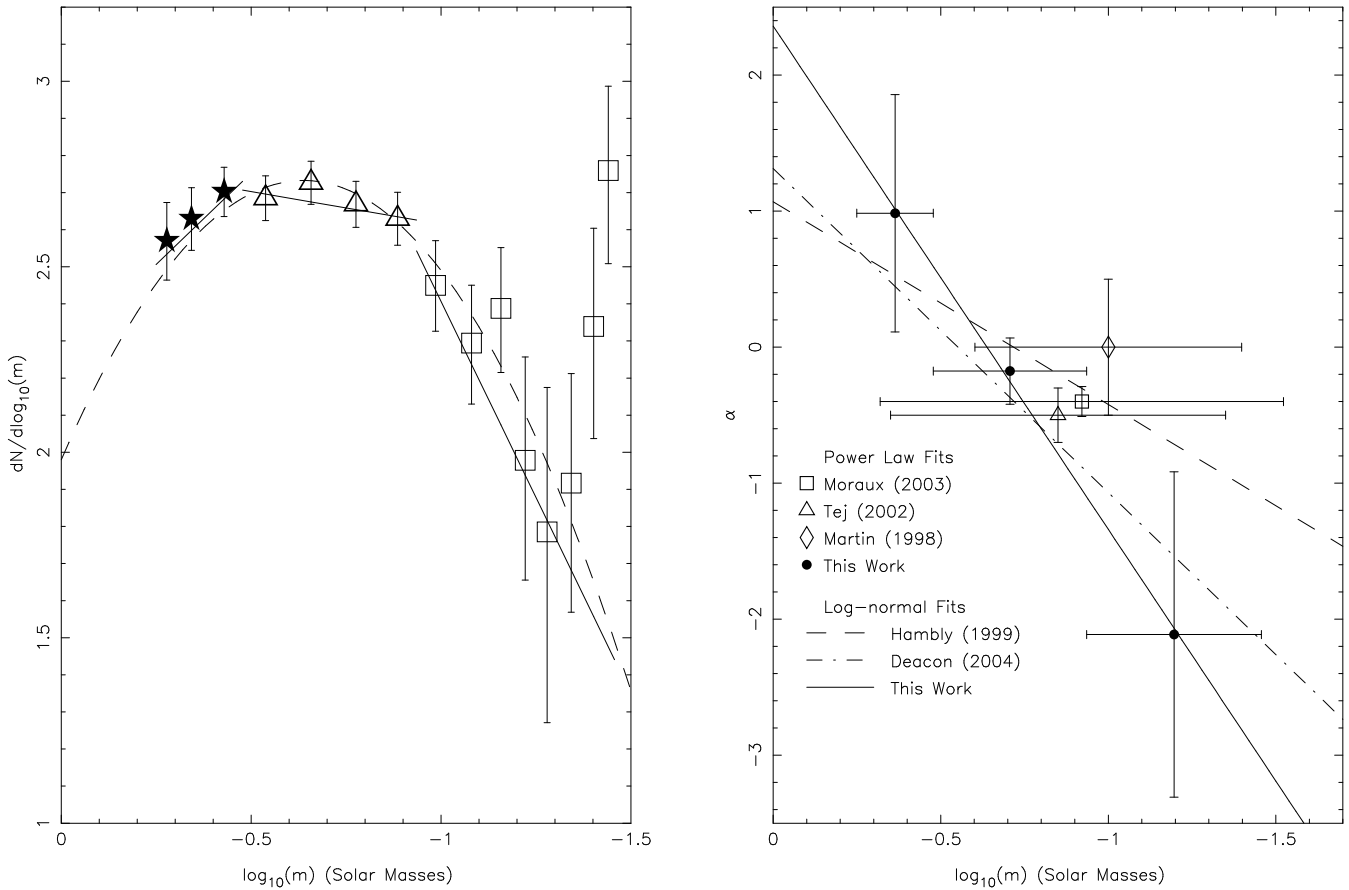


Figure 8. *Left:* The Pleiades mass function for all candidates extracted from the UKIDSS GCS DR1. We have assumed a distance of 130 pc and an age of 120 Myr for the Pleiades cluster. The NextGen and DUSTY models were used to transform magnitudes into masses. Error bars are Gehrels errors. Three power law segments (solid lines) were fit to the mass function with α parameters as follows: 0.98 ± 0.87 in the $0.563\text{--}0.333 M_{\odot}$ mass range (filled circles), -0.18 ± 0.24 for $0.333\text{--}0.116 M_{\odot}$ (star symbols), and -2.11 ± 1.20 over $0.116\text{--}0.035 M_{\odot}$ (open squares). The lognormal function (dashed lines) has the following parameters $a_0 = 1.99$, $a_1 = -2.37$, and $a_2 = -1.89$ (using the definition in Section 6.2). *Right:* The α -plot for the Pleiades mass function. The filled circles represent the three power law segments from our study and the solid line the lognormal function fit to the mass function. Other symbols and lines depict previous studies: Martín et al. (1998, ; open diamond), Hamby et al. (1999, dashed line), Martín et al. (1998, open diamond), Tej et al. (2002, open triangle), Moraux et al. (2003, open square), and Deacon & Hamby (2004, dot-dashed line). Vertical segments represent the error on the α index whereas the horizontal bars represent the range in mass where the α index is valid.

Hamby N. C., Hodgkin S. T., Cossburn M. R., Jameson R. F., 1999, *MNRAS*, 303, 835
 Hamby N. C., Steele I. A., Hawkins M. R. S., Jameson R. F., 1995, *MNRAS*, 273, 505
 Hewett P. C., Warren S. J., Leggett S. K., Hodgkin S. T., 2006, *MNRAS*, 367, 454
 Hillenbrand L. A., White R. J., 2004, *ApJ*, 604, 741
 Irwin M., Lewis J., 2001, *New Astronomy Review*, 45, 105
 Irwin M. J., et al. eds, *Optimizing Scientific Return for Astronomy through Information Technologies*. Edited by Quinn, Peter J.; Bridger, Alan. *Proceedings of the SPIE*, Volume 5493, pp. 411–422 (2004). VISTA data flow system: pipeline processing for WFCAM and VISTA. pp 411–422
 Jameson R. F., Dobbie P. D., Hodgkin S. T., Pinfield D. J., 2002, *MNRAS*, 335, 853
 Jameson R. F., Skillen I., 1989, *MNRAS*, 239, 247
 Joergens V., 2006, *A&A*, 446, 1165
 Johnson H. L., 1957, *ApJ*, 126, 121
 Jones B. F., Stauffer J. R., 1991, *AJ*, 102, 1080
 Kenyon M. J., Jeffries R. D., Naylor T., Oliveira J. M., Mated P. F. L., 2005, *MNRAS*, 356, 89

Kraus A. L., White R. J., Hillenbrand L. A., 2006, *ApJ*, 649, 306
 Lawrence A., et al. 2006, arXiv:astro-ph/0604426
 Lodieu N., Hamby N. C., Jameson R. F., 2006, *MNRAS*, 373, 95
 Lodieu N., Hamby N. C., Jameson R. F., Hodgkin S. T., Carraro G., Kendall T. R., 2007, *MNRAS*, 374, 372
 Lucas P. W., Roche P. F., 2000, *MNRAS*, 314, 858
 Luhman K. L., 1999, *ApJ*, 525, 466
 Luhman K. L., 2004, *ApJ*, 617, 1216
 Luhman K. L., Rieke G. H., Lada C. J., Lada E. A., 1998, *ApJ*, 508, 347
 Luhman K. L., Rieke G. H., Young E. T., Cotera A. S., Chen H., Rieke M. J., Schneider G., Thompson R. I., 2000, *ApJ*, 540, 1016
 Martín E. L., Barrado y Navascués D., Baraffe I., Bouy H., Dahm S., 2003, *ApJ*, 594, 525
 Martín E. L., Brandner W., Bouvier J., Luhman K. L., Stauffer J., Basri G., Zapatero Osorio M. R., Barrado y Navascués D., 2000, *ApJ*, 543, 299
 Martín E. L., Zapatero Osorio M. R., Rebolo R., 1998, in *ASP Conf. Ser. 134: “Brown Dwarfs and Extrasolar Planets”*, eds. R. Rebolo, E. L. Martín, and M. R. Zapatero Osorio *The Substellar Initial Mass Function in the Pleiades*. p. 507

- Maxted P. F. L., Jeffries R. D., 2005, MNRAS, 362, L45
Moraux E., Bouvier J., Stauffer J. R., 2001, A&A, 367, 211
Moraux E., Bouvier J., Stauffer J. R., Cuillandre J.-C., 2003, A&A, 400, 891
Moraux E., Kroupa P., Bouvier J., 2004, A&A, 426, 75
Muench A. A., Lada E. A., Lada C. J., Alves J., 2002, ApJ, 573, 366
Muench A. A., et al. 2003, AJ, 125, 2029
O'dell M. A., Hendry M. A., Collier Cameron A., 1994, MNRAS, 268, 181
Palla F., Baraffe I., 2005, A&A, 432, L57
Pinfield D. J., Dobbie P. D., Jameson R. F., Steele I. A., Jones H. R. A., Katsiyannis A. C., 2003, MNRAS, 342, 1241
Pinfield D. J., Hodgkin S. T., Jameson R. F., Cossburn M. R., Hambly N. C., Devereux N., 2000, MNRAS, 313, 347
Rebolo R., Martín E. L., Magazzù A., 1992, ApJL, 389, L83
Reid I. N., et al. 1991, PASP, 103, 661
Robichon N., Arenou F., Mermilliod J.-C., Turon C., 1999, A&A, 345, 471
Salpeter E. E., 1955, ApJ, 121, 161
Schwartz M. J., Becklin E. E., 2005, AJ, 130, 2352
Slesnick C. L., Hillenbrand L. A., Carpenter J. M., 2004, ApJ, 610, 1045
Southworth J., Maxted P. F. L., Smalley B., 2005, A&A, 429, 645
Stauffer J. R., Schultz G., Kirkpatrick J. D., 1998, ApJL, 499, 219
Tej A., Sahu K. C., Chandrasekhar T., Ashok N. M., 2002, ApJ, 578, 523
Vrba F. J., et al. 2004, AJ, 127, 2948
Warren S. J., et al. 2007, MNRAS, 375, 213
Zapatero Osorio M. R., Rebolo R., Martín E. L., Hodgkin S. T., Cossburn M. R., Magazzù A., Steele I. A., Jameson R. F., 1999, A&AS, 134, 537

**APPENDIX A: TABLE OF OF HIGH PROBABILITY
PROPER MOTION MEMBERS AND NEW
PHOTOMETRIC CANDIDATES IN THE PLEIADES FROM
THE UKIDSS GCS DR1.**

**APPENDIX B: TABLE OF FAINT PROPER MOTION
NON-MEMBERS IN THE PLEIADES EXTRACTED FROM
THE UKIDSS GCS DR1**

**APPENDIX C: TABLE OF FAINT PHOTOMETRIC
NON-MEMBERS IN THE PLEIADES EXTRACTED FROM
THE UKIDSS GCS DR1**

**APPENDIX D: TABLE OF FAINT YJ CANDIDATES IN
THE PLEIADES EXTRACTED FROM THE UKIDSS GCS
DR1.**

**APPENDIX E: TABLE OF FAINT JK CANDIDATES IN
THE PLEIADES EXTRACTED FROM THE UKIDSS GCS
DR1.**

**APPENDIX F: TABLE OF LOW-MASS MULTIPLE
SYSTEM CANDIDATES IN THE PLEIADES EXTRACTED
FROM THE UKIDSS GCS DR1.**

Table A1. Near-infrared (*ZYJHK*) photometry for 43 high probability members and 73 new photometric candidates in the Pleiades open clusters. All sources are fainter than $Z = 16$ mag, corresponding to masses below $0.1 M_{\odot}$ according to theoretical models. This table lists the equatorial coordinates (in J2000), magnitudes from the GCS, PMs, membership probabilities when available, membership status, and names from the literature for each source. (memb stands for high probability ($p \geq 0.6$) PM members whereas cand qualify new photometric candidates.

R.A.	Dec.	<i>Z</i>	<i>Y</i>	<i>J</i>	<i>H</i>	<i>K</i>	$\mu_{\alpha} \cos \delta$	μ_{δ}	Prob	Memb?	Other name
03 40 35.50	23 13 07.4	17.908	16.811	16.073	15.499	15.004	19.61	-35.45	—	cand	UGCS-PI-1
03 40 39.46	23 26 34.8	16.167	15.563	15.020	14.455	14.062	16.55	-41.62	—	cand	NoName
03 40 52.79	25 24 43.4	19.156	18.009	17.115	16.423	15.853	—	—	—	cand	UGCS-PI-2
03 40 55.30	25 34 57.4	17.381	16.464	15.817	15.187	14.727	21.07	-58.68	—	cand	UGCS-PI-3
03 41 30.36	25 17 06.0	16.555	15.821	15.240	14.674	14.297	11.31	-40.18	0.849	memb	UGCS-PI-4
03 41 33.90	23 11 44.9	16.134	15.557	15.029	14.501	14.150	37.63	-33.57	—	cand	HHJ12
03 41 37.74	23 04 32.7	17.929	17.005	16.315	15.658	15.208	—	—	—	cand	UGCS-PI-5
03 41 40.90	25 54 24.1	16.829	15.900	15.173	14.562	14.114	23.78	-37.48	0.915	memb	CFHT-PLIZ4
03 41 43.72	23 07 59.8	16.340	15.654	15.072	14.522	14.105	17.71	-45.66	—	cand	UGCS-PI-6
03 41 54.16	23 05 04.8	17.336	16.297	15.499	14.912	14.385	10.66	-24.90	—	cand	MHOBD3
03 42 05.74	23 07 14.4	16.654	15.911	15.343	14.769	14.344	16.53	-36.85	—	cand	UGCS-PI-7
03 42 07.99	22 39 33.5	18.718	17.398	16.515	15.809	15.192	—	—	—	cand	int-pl-IZ-76
03 42 47.29	23 00 40.4	17.009	16.194	15.554	14.965	14.553	12.99	-48.09	—	cand	UGCS-PI-8
03 42 59.92	22 42 51.5	16.067	15.267	14.666	14.109	13.708	25.70	-41.46	0.860	memb	UGCS-PI-9
03 43 11.76	25 31 32.0	16.020	15.352	14.778	14.233	13.897	9.82	-49.41	—	cand	UGCS-PI-10
03 43 22.55	23 00 56.5	16.141	15.457	14.899	14.354	13.985	10.54	-33.85	—	cand	UGCS-PI-11
03 43 34.48	25 57 30.6	16.471	15.605	14.889	14.323	13.897	9.23	-40.49	—	cand	UGCS-PI-12
03 43 56.00	25 36 25.3	16.702	15.888	15.300	14.693	14.320	11.28	-43.18	0.805	memb	UGCS-PI-13
03 44 22.44	23 39 01.4	19.013	17.739	16.885	16.249	15.647	28.82	-42.67	0.647	memb	Roque5
03 44 23.24	25 38 44.9	16.288	15.349	14.692	14.133	13.744	16.08	-28.17	—	cand	BRB4
03 44 25.58	22 40 07.9	16.194	15.511	14.944	14.383	13.989	16.23	-30.26	0.658	memb	UGCS-PI-14
03 44 32.33	25 25 18.0	16.945	16.120	15.460	14.884	14.466	20.34	-37.19	0.949	memb	cfht10
03 44 34.30	23 51 24.6	16.799	16.016	15.444	14.858	14.453	33.10	-39.85	—	cand	UGCS-PI-15
03 44 35.16	25 13 42.8	17.567	16.482	15.651	14.979	14.439	21.14	-39.28	0.952	memb	CFHTPLIZ9,CFHT-PI-16
03 44 35.90	23 34 42.0	16.224	15.551	14.991	14.369	13.973	21.72	-32.67	0.840	memb	HHJ5
03 44 53.12	23 34 22.9	17.223	16.356	15.740	15.110	14.695	21.30	-31.20	0.754	memb	UGCS-PI-16
03 45 04.41	24 15 16.6	20.325	18.895	17.768	16.943	16.318	—	—	—	cand	UGCS-PI-17
03 45 08.69	24 24 09.4	16.345	15.700	15.129	14.552	14.213	18.35	-52.13	—	cand	UGCS-PI-18
03 45 09.46	23 58 44.7	16.820	16.099	15.417	14.830	14.382	30.39	-47.73	—	cand	PPL2
03 45 31.37	24 52 47.5	17.246	16.226	15.471	14.842	14.329	19.65	-30.23	—	cand	IPMBD29
03 45 35.69	24 24 34.2	16.487	15.726	15.154	14.577	14.186	9.53	-47.20	—	cand	UGCS-PI-19
03 45 37.76	23 43 50.1	16.129	15.320	14.710	14.149	13.731	28.02	-41.71	0.696	memb	UGCS-PI-20
03 45 41.27	23 54 09.8	17.039	16.055	15.345	14.761	14.281	15.29	-42.72	0.931	memb	Roque15
03 45 42.33	24 04 11.2	16.420	15.757	15.203	14.624	14.252	14.24	-40.62	0.931	memb	UGCS-PI-21
03 45 50.42	22 36 05.6	17.593	16.734	16.039	15.488	15.017	20.35	-39.71	0.956	memb	BPL78
03 45 50.66	24 09 03.5	17.352	16.451	15.692	15.060	14.569	17.66	-53.57	—	cand	roque13
03 45 53.20	25 12 55.8	17.481	16.671	15.998	15.346	14.935	—	—	—	cand	BPL81
03 45 54.96	23 33 57.9	17.032	16.209	15.560	15.005	14.550	16.40	-39.61	0.952	memb	UGCS-PI-22
03 46 02.52	23 45 33.2	18.077	17.254	16.460	15.458	15.012	—	—	—	cand	UGCS-PI-23
03 46 03.75	23 44 35.6	18.074	17.137	16.410	15.528	15.040	—	—	—	cand	UGCS-PI-24
03 46 08.02	23 45 35.5	18.787	17.829	16.857	15.832	15.324	—	—	—	cand	UGCS-PI-25
03 46 10.23	21 52 55.8	16.115	15.233	14.573	13.949	13.548	36.60	-41.94	—	cand	UGCS-PI-26
03 46 14.06	23 21 56.5	17.005	16.220	15.574	15.013	14.589	16.37	-27.55	—	cand	UGCS-PI-27
03 46 22.25	23 52 26.6	17.013	16.179	15.526	14.879	14.440	16.52	-39.19	0.953	memb	UGCS-PI-28
03 46 23.12	24 20 36.1	18.081	17.027	16.233	15.636	15.134	—	—	—	cand	BPL100
03 46 26.09	24 05 09.5	16.660	15.824	15.127	14.561	14.097	17.99	-40.76	0.957	memb	IPMBD25
03 46 27.10	21 48 22.6	19.764	18.557	17.387	16.557	15.845	—	—	—	cand	UGCS-PI-29
03 46 32.13	24 23 14.6	19.104	17.932	17.030	16.345	15.840	—	—	—	cand	UGCS-PI-30
03 46 34.25	23 50 03.7	19.799	18.422	17.483	16.644	16.070	17.97	-38.98	0.686	memb	UGCS-PI-31
03 46 34.99	23 31 14.4	18.353	17.242	16.406	15.818	15.301	—	—	—	cand	UGCS-PI-32
03 46 35.36	23 57 07.4	16.768	15.943	15.346	14.756	14.384	16.65	-42.51	0.944	memb	UGCS-PI-33
03 46 40.94	22 22 38.2	19.193	18.048	16.910	16.151	15.495	—	—	—	cand	UGCS-PI-34
03 46 48.56	23 09 57.6	16.434	15.709	15.087	14.515	14.078	20.25	-36.11	—	cand	UGCS-PI-35
03 46 50.03	24 00 23.6	17.295	16.335	15.594	14.987	14.502	18.70	-36.10	0.943	memb	UGCS-PI-36
03 46 51.82	23 23 09.4	19.574	18.324	17.182	16.399	15.647	—	—	—	cand	UGCS-PI-37
03 46 52.97	24 15 07.8	16.271	15.623	15.058	14.480	14.125	19.58	-42.79	—	cand	MHO7
03 46 55.48	23 11 16.1	20.298	18.965	17.886	17.117	16.426	—	—	—	cand	UGCS-PI-38
03 47 01.85	24 13 28.1	16.124	15.496	14.931	14.374	14.022	18.48	-43.76	—	cand	MHO10
03 47 04.41	24 47 27.4	20.645	19.401	18.057	17.099	16.504	—	—	—	cand	UGCS-PI-39
03 47 05.71	24 40 03.6	16.905	16.048	15.447	14.850	14.425	25.97	-35.30	—	cand	BPL124
03 47 05.79	23 45 34.7	16.168	15.444	14.883	14.314	13.972	19.17	-42.39	0.950	memb	UGCS-PI-40

R.A.	Dec.	Z	Y	J	H	K	$\mu_\alpha \cos \delta$	μ_δ	Prob	Memb?	Other name
03 47 10.65	23 58 16.4	16.041	15.466	14.887	14.340	13.990	16.16	-33.75	0.886	memb	UGCS-PI-41
03 47 11.79	24 13 31.3	16.182	15.444	14.805	14.234	13.860	9.97	-28.34	—	cand	MHO11
03 47 17.92	24 22 31.7	18.033	16.955	16.192	15.581	15.093	—	—	—	cand	Teide1
03 47 18.10	24 45 14.6	19.060	17.973	17.107	16.303	15.678	—	—	—	cand	UGCS-PI-42
03 47 27.72	22 09 38.6	17.332	16.426	15.733	15.169	14.726	9.37	-38.49	—	cand	MHOBD5
03 47 29.59	23 52 49.4	16.294	15.563	15.003	14.425	14.049	14.04	-37.97	—	cand	UGCS-PI-43
03 47 39.02	24 36 22.2	17.068	16.158	15.537	14.954	14.530	20.06	-39.23	0.956	memb	BRB12
03 47 46.77	25 35 16.6	20.340	18.479	17.438	16.673	16.142	—	—	—	cand	UGCS-PI-44
03 47 48.91	24 17 06.6	20.153	19.148	17.841	17.014	16.406	—	—	—	cand	UGCS-PI-45
03 47 49.45	23 31 52.9	17.057	16.199	15.615	15.022	14.606	34.87	-44.39	—	cand	UGCS-PI-46
03 47 50.41	23 54 47.9	18.087	17.007	16.300	15.589	15.078	—	—	—	cand	NoName
03 47 58.03	22 06 50.9	16.686	15.892	15.282	14.721	14.327	24.86	-32.10	—	cand	bpl163
03 47 59.73	22 36 01.9	17.981	16.986	16.206	15.588	15.106	—	—	—	cand	int-pl-IZ-33
03 48 04.67	23 39 30.2	16.964	15.939	15.294	14.683	14.256	21.59	-29.33	—	cand	PPL15
03 48 14.30	24 15 50.6	16.582	15.828	15.226	14.675	14.253	10.53	-52.30	—	cand	BPL169
03 48 27.36	23 46 16.3	20.616	19.569	18.148	17.346	16.490	—	—	—	cand	UGCS-PI-47
03 48 30.29	24 18 00.3	20.176	19.108	17.804	16.960	16.373	—	—	—	cand	UGCS-PI-48
03 48 31.52	24 34 37.3	19.163	17.784	16.727	15.964	15.343	18.05	-39.05	0.687	memb	BRB16
03 48 38.37	22 33 51.8	17.262	16.416	15.707	15.162	14.713	8.64	-50.82	—	cand	UGCS-PI-49
03 48 44.69	24 37 23.5	16.208	15.478	14.916	14.396	13.989	23.06	-35.91	0.910	memb	CFHT5
03 48 55.65	24 21 40.2	16.160	15.535	14.953	14.391	14.031	19.28	-39.16	—	cand	HHJ8
03 49 04.86	23 33 39.3	17.133	16.229	15.593	15.037	14.573	9.55	-35.28	—	cand	Roque47
03 49 05.18	22 04 52.7	16.624	15.857	15.264	14.724	14.331	12.38	-53.26	—	cand	UGCS-PI-50
03 49 12.51	24 11 12.8	18.376	17.249	16.413	15.776	15.254	—	—	—	cand	BPL201
03 49 15.12	24 36 22.5	16.797	15.947	15.367	14.846	14.418	17.46	-42.66	0.946	memb	BRB10
03 49 41.21	22 56 40.6	16.218	15.561	15.008	14.415	14.072	20.05	-42.05	0.950	memb	BPL213
03 49 43.17	24 39 46.5	16.325	15.616	15.067	14.507	14.100	18.57	-34.64	0.923	memb	BPL215
03 49 52.43	24 03 43.0	16.028	15.423	14.871	14.330	13.947	23.88	-39.12	—	cand	UGCS-PI-51
03 49 56.81	24 59 07.1	16.412	15.744	15.142	14.591	14.180	17.87	-40.58	0.957	memb	BPL218
03 50 08.27	25 30 51.7	19.578	18.202	17.248	16.579	16.007	—	—	—	cand	UGCS-PI-52
03 50 13.39	23 59 29.8	20.404	19.093	17.845	16.892	16.205	—	—	—	cand	UGCS-PI-53
03 50 16.09	24 08 34.8	19.872	18.458	17.338	16.664	16.077	15.01	-36.98	0.619	memb	Roque30
03 50 19.15	24 16 34.0	16.370	15.687	15.081	14.547	14.174	17.25	-44.27	0.926	memb	BPL228
03 50 22.01	23 55 30.4	17.248	16.292	15.692	15.077	14.673	29.42	-25.82	—	cand	UGCS-PI-54
03 51 05.97	24 36 16.9	17.082	16.231	15.654	15.122	14.703	10.72	-34.15	0.664	memb	CFHT-PLIZ1
03 51 26.60	22 48 46.0	18.839	99.999	16.661	15.898	15.309	—	—	—	cand	UGCS-PI-55
03 51 38.96	24 30 44.8	18.723	17.316	16.408	15.702	15.148	18.71	-41.66	0.751	memb	UGCS-PI-56
03 51 42.34	25 57 25.6	16.116	15.540	14.967	14.376	14.006	24.40	-26.00	—	cand	UGCS-PI-57
03 51 44.94	23 26 39.3	17.732	16.805	16.031	15.401	14.971	13.26	-38.62	0.912	memb	CFHTPLIZ10,BPL240
03 51 59.27	23 17 17.8	17.351	16.490	15.811	15.245	14.859	23.58	-35.81	0.898	memb	UGCS-PI-58
03 52 02.10	23 15 45.4	18.648	17.523	16.700	16.032	15.474	20.83	-37.87	0.737	memb	BPL249
03 52 05.82	24 17 31.1	16.470	15.771	15.186	14.614	14.251	13.32	-41.59	0.909	memb	NoName
03 52 06.72	24 16 00.5	17.040	16.168	15.523	14.967	14.503	13.37	-48.12	0.638	memb	CFHT-PLIZ3,CFHT-PI-13_Teide2
03 52 55.92	24 57 41.8	16.279	15.671	15.099	14.518	14.148	25.39	-41.63	0.870	memb	BPL275
03 53 23.13	23 19 20.4	17.768	16.798	15.963	15.327	14.818	—	—	—	cand	BPL283
03 53 24.24	25 14 37.7	16.722	15.951	15.332	14.772	14.381	13.82	-45.98	—	cand	UGCS-PI-59
03 54 05.35	23 33 59.3	18.668	17.505	16.666	15.961	15.426	14.61	-39.84	0.717	memb	CFHTPLIZ20,CFHT-PI-25_BPL
03 54 15.28	25 09 52.2	17.828	16.913	16.164	15.550	15.071	16.71	-20.27	—	cand	BPL306
03 54 31.48	22 39 01.6	16.552	15.766	15.173	14.571	14.187	15.83	-40.39	0.948	memb	UGCS-PI-60
03 55 12.61	23 17 37.3	17.759	16.765	15.962	15.330	14.835	—	—	—	cand	CFHT15
03 55 18.11	24 17 05.7	16.242	15.660	15.100	14.526	14.185	21.11	-22.06	—	cand	BPL326
03 55 27.06	25 14 45.8	16.048	15.299	14.643	14.046	13.659	22.98	-39.83	0.936	memb	BPL328
03 55 47.14	25 14 39.6	17.188	16.421	15.772	15.201	14.797	8.24	-29.85	—	cand	UGCS-PI-61
03 55 47.45	22 50 50.2	19.883	18.435	17.421	16.667	16.088	—	—	—	cand	UGCS-PI-62
03 56 11.38	25 03 36.5	16.606	15.895	15.229	14.675	14.323	22.99	-41.23	0.932	memb	BPL334

Table B1. List of 53 high probability and new photometric candidates classified as PM non-members based on their PM derived from the 2MASS vs GCS cross-correlation. This table lists the equatorial coordinates (in J2000), magnitudes from the GCS, and PMs for each source.

R.A.	Dec.	<i>Z</i>	<i>Y</i>	<i>J</i>	<i>H</i>	<i>K</i>	$\mu_{\alpha} \cos \delta$	μ_{δ}
03 41 45.82	23 14 26.1	16.003	15.484	14.953	14.256	13.957	14.50	-14.79
03 42 04.72	23 29 04.2	16.183	15.652	15.107	14.438	14.118	-6.28	-11.03
03 42 10.17	22 48 44.6	17.200	16.245	15.528	14.893	14.443	19.91	-82.78
03 43 53.05	23 21 50.2	16.062	15.560	15.019	14.336	14.015	-23.88	-14.35
03 44 09.39	23 17 07.2	16.319	15.751	15.168	14.586	14.233	-16.32	4.32
03 44 10.08	22 43 57.8	16.275	15.691	15.175	14.569	14.246	-3.75	-12.96
03 44 33.80	22 42 49.2	16.485	15.857	15.333	14.709	14.331	2.88	18.30
03 45 21.12	21 46 17.5	16.262	15.793	15.149	14.562	14.230	-14.43	-38.91
03 45 22.14	21 52 40.0	16.220	15.655	15.115	14.550	14.191	4.94	-66.09
03 45 28.34	23 48 09.6	16.983	16.259	15.577	14.721	14.285	21.69	-0.94
03 45 29.86	22 24 14.6	16.335	15.699	15.176	14.555	14.221	40.98	-85.07
03 45 34.50	23 41 43.5	16.959	16.237	15.608	14.846	14.430	-17.30	-14.64
03 45 36.44	24 18 15.4	16.079	15.561	15.037	14.415	14.095	8.91	6.78
03 45 36.85	23 44 47.8	16.669	16.245	15.423	14.641	14.244	7.10	12.74
03 45 37.25	23 49 21.0	16.279	15.725	15.116	14.203	13.866	-21.11	9.22
03 45 43.12	25 40 23.1	16.150	14.905	13.924	13.220	12.638	-102.76	-38.74
03 45 49.90	23 45 59.8	16.124	15.484	14.810	13.887	13.578	6.17	7.13
03 46 08.22	23 21 38.7	17.011	16.367	15.720	14.986	14.614	-14.77	-6.54
03 46 14.47	22 20 51.1	16.639	15.992	15.456	14.964	14.587	72.99	-67.54
03 46 26.76	24 49 18.1	16.210	15.604	15.109	14.497	14.196	-30.58	-28.37
03 46 33.00	23 38 00.9	16.537	15.946	15.377	14.425	14.120	-9.39	7.18
03 46 34.16	23 25 12.5	16.210	15.672	15.079	14.377	14.041	9.28	4.89
03 46 36.83	23 33 01.8	16.659	15.959	15.359	14.488	14.113	-6.73	-11.83
03 46 44.04	23 38 13.5	17.114	16.411	15.786	14.916	14.564	20.68	-7.25
03 46 50.99	25 40 44.6	16.230	15.655	15.164	14.450	14.174	-2.52	-13.87
03 46 52.29	21 47 43.1	16.695	15.996	15.417	14.783	14.401	22.89	-8.81
03 47 06.65	24 45 47.4	16.051	15.414	14.968	14.414	14.093	75.15	40.22
03 47 08.31	22 33 10.0	16.500	15.881	15.332	14.804	14.422	-9.26	17.59
03 47 13.69	23 46 28.4	16.347	15.706	15.221	14.656	14.329	-14.07	7.48
03 47 36.27	24 28 50.1	16.049	15.482	14.967	14.279	13.929	-9.18	-5.59
03 48 23.62	24 22 35.2	16.151	15.466	14.890	14.299	13.938	-15.18	-6.70
03 48 36.30	23 33 25.3	16.054	15.512	15.035	14.472	14.147	-16.67	-28.01
03 48 48.46	21 59 00.3	16.514	15.869	15.332	14.779	14.470	-18.96	3.15
03 49 11.59	24 26 17.5	16.030	15.415	14.930	14.412	14.078	35.55	-81.10
03 49 12.12	23 12 55.9	16.821	16.077	15.427	14.815	14.414	67.42	4.88
03 50 03.94	24 56 02.9	16.179	15.630	15.102	14.494	14.124	-6.50	-42.38
03 50 15.55	26 06 30.1	16.821	16.081	15.407	14.810	14.390	45.38	-60.60
03 51 04.04	24 32 57.9	16.032	15.447	14.981	14.371	14.053	83.02	-39.72
03 51 09.72	25 18 52.4	16.705	15.956	15.399	14.872	14.515	-8.24	-31.78
03 51 10.52	22 48 14.5	16.717	16.031	15.451	14.754	14.406	-9.03	-22.58
03 51 27.90	22 48 12.9	16.073	15.332	14.720	14.081	13.693	24.54	5.16
03 51 38.18	23 03 11.2	16.859	16.116	15.533	14.952	14.580	-8.79	-0.54
03 52 07.88	23 59 13.1	16.135	15.284	14.620	14.057	13.620	22.45	-86.80
03 52 17.49	22 51 01.9	16.583	15.973	15.412	14.759	14.389	-8.79	3.35
03 53 48.72	25 04 20.1	16.729	16.213	15.240	15.098	14.797	3.44	-18.98
03 53 59.92	23 41 00.3	16.175	15.572	15.052	14.450	14.115	-5.34	-13.33
03 54 17.46	23 11 56.9	16.131	15.574	15.017	14.432	14.088	-9.91	5.36
03 54 39.33	23 03 12.4	16.394	15.588	14.992	14.444	14.053	10.21	-1.55
03 54 40.56	23 42 23.7	16.106	15.547	15.060	14.425	14.155	7.21	4.10
03 54 46.11	23 00 20.6	17.017	16.309	15.704	15.103	14.741	-26.85	-1.64
03 54 54.51	22 50 21.5	16.403	15.752	15.216	14.651	14.338	-0.85	-0.54
03 55 14.72	22 42 08.5	16.637	15.962	15.384	14.731	14.381	23.51	-12.75
03 55 30.07	23 54 53.5	16.466	15.829	15.296	14.788	14.421	-7.60	-1.05

Table C1. List of 24 high probability and new photometric candidates classified as photometric non-members from their location in several colour-magnitude diagrams. This table lists the equatorial coordinates (in J2000), magnitudes from the GCS, and PMs for each source.

R.A.	Dec.	<i>Z</i>	<i>Y</i>	<i>J</i>	<i>H</i>	<i>K</i>	$\mu_{\alpha} \cos \delta$	μ_{δ}
03 41 31.46	23 05 12.3	18.520	19.416	16.757	16.269	16.179	—	—
03 41 36.55	22 41 01.7	16.248	15.641	15.136	14.585	14.250	35.42	-33.96
03 42 27.94	25 25 20.0	19.822	19.332	17.711	17.062	16.874	—	—
03 43 12.21	23 09 16.6	18.540	17.489	16.670	16.022	15.589	—	—
03 43 52.03	22 55 24.5	18.874	17.727	16.970	16.272	15.782	—	—
03 44 12.68	25 24 35.1	18.058	17.144	16.455	15.949	15.527	—	—
03 45 33.16	25 34 30.0	18.079	17.112	16.422	15.843	15.381	—	—
03 46 04.92	22 15 40.2	17.386	16.555	15.899	15.246	15.018	—	—
03 47 46.15	25 21 42.3	19.444	18.280	17.382	16.876	16.331	—	—
03 48 19.02	24 25 12.8	17.666	16.597	15.972	15.375	14.951	19.35	-34.91
03 48 49.03	24 20 25.3	19.165	18.125	17.229	16.543	16.037	—	—
03 48 58.61	23 37 03.9	19.567	18.221	17.389	16.735	16.231	—	—
03 49 21.17	23 34 02.0	18.409	17.353	16.637	16.030	15.530	—	—
03 49 48.77	23 42 59.4	19.147	18.083	17.235	16.608	16.099	—	—
03 49 51.23	25 26 06.6	19.698	18.476	17.608	17.059	16.494	—	—
03 50 15.33	24 35 40.4	16.124	15.521	15.070	14.470	14.175	8.32	-22.94
03 51 37.72	25 42 46.6	19.070	17.672	16.338	15.428	14.640	—	—
03 51 59.93	23 24 25.6	19.627	18.336	17.387	16.694	16.250	—	—
03 52 13.44	24 28 52.3	20.026	18.527	17.772	17.224	16.643	—	—
03 52 46.44	24 24 16.9	19.536	18.447	17.533	16.955	16.317	—	—
03 53 26.55	24 46 44.9	16.022	15.487	14.996	14.417	14.107	-2.92	-47.58
03 54 55.92	24 37 43.0	20.857	19.356	18.324	17.897	17.734	—	—
03 55 39.58	24 12 51.1	20.442	19.165	17.853	17.285	16.634	—	—
03 55 42.01	22 57 01.4	18.624	17.246	15.954	14.995	14.189	—	—

Table D1. Near-infrared (*ZYJHK*) photometry for 35 photometric candidates with no *Z* detection and selected from the (*Y* − *J*, *Y*) CMD. This table lists the equatorial coordinates (in J2000), the magnitudes from the GCS, their PMs, and their membership status (Memb≡photometric and PM member; cand≡photometric candidate in all diagrams; photNM≡photometric non-member; PM_NM≡PM non-member; dubious≡likely false detection).

R.A.	Dec.	<i>Y</i>	<i>J</i>	<i>H</i>	<i>K</i>	$\mu_{\alpha} \cos \delta$	μ_{δ}	Memb?
03 42 14.28	22 43 02.5	19.977	18.526	18.017	17.482	—	—	photNM
03 42 59.30	25 37 39.1	19.727	18.241	17.367	16.647	—	—	Memb
03 44 30.52	24 21 17.4	19.458	18.396	17.684	17.301	—	—	dubious
03 44 31.28	25 35 14.8	19.336	18.282	17.394	16.658	13.96	−39.80	Memb
03 44 47.32	24 21 35.8	19.553	18.411	17.477	16.898	—	—	photNM
03 45 01.81	24 04 17.8	20.431	19.025	18.800	18.030	—	—	dubious
03 45 11.56	23 25 35.1	20.233	18.911	18.104	17.485	—	—	photNM
03 45 33.30	23 34 34.3	19.576	18.130	17.182	16.485	13.67	−9.64	PM_NM
03 45 35.06	21 56 22.3	19.364	18.168	17.575	17.114	−11.06	1.62	PM_NM
03 46 27.94	23 42 38.9	19.681	18.570	17.708	17.437	−8.48	−26.82	PM_NM
03 46 29.11	22 59 47.7	18.992	17.740	16.768	15.924	—	—	Memb
03 46 51.05	22 34 28.9	19.779	18.581	18.075	17.292	—	—	dubious
03 47 33.15	23 36 32.6	19.210	17.894	18.063	16.898	—	—	dubious
03 47 38.47	23 56 27.7	19.827	18.334	17.435	16.661	—	—	Memb
03 47 44.16	24 57 24.1	20.088	18.692	17.877	17.246	—	—	photNM
03 47 46.52	24 55 46.6	19.426	18.247	17.398	16.590	—	—	Memb
03 48 05.47	21 57 31.2	20.043	18.753	17.929	17.311	—	—	photNM
03 48 15.64	25 50 09.0	19.785	18.497	17.631	16.758	25.82	−44.45	Memb
03 48 39.56	23 56 11.7	20.619	19.223	18.728	18.153	—	—	photNM
03 49 17.16	23 19 42.8	19.726	18.548	17.657	16.738	—	—	Memb
03 49 28.92	23 22 49.1	19.975	18.385	18.095	16.706	—	—	dubious
03 50 15.96	24 23 28.7	20.017	18.711	17.774	16.887	—	—	Memb
03 50 39.54	25 02 54.7	19.677	18.208	17.331	16.565	—	—	Memb
03 51 29.47	24 00 37.4	19.610	18.412	17.463	16.696	25.57	−44.48	Memb
03 51 41.62	25 55 45.4	20.484	19.107	18.453	18.047	—	—	photNM
03 52 05.33	25 37 34.0	18.874	17.699	17.937	17.520	—	—	dubious
03 52 27.18	23 12 08.1	19.216	18.005	17.069	16.351	1.58	−9.79	PM_NM
03 52 34.75	22 56 04.5	19.524	18.437	17.554	17.070	—	—	photNM
03 52 39.15	24 46 29.5	19.189	18.069	17.098	16.486	−1.52	−33.36	Memb
03 52 59.62	24 42 35.6	20.584	19.093	18.681	18.220	—	—	dubious
03 53 18.93	23 12 39.1	19.959	18.327	17.604	16.880	—	—	photNM
03 54 10.28	23 41 40.1	19.156	18.124	17.141	16.377	7.50	−27.69	Memb
03 54 30.49	25 11 21.8	19.884	18.657	18.116	17.519	—	—	photNM
03 54 49.89	24 16 23.4	19.451	18.279	18.241	17.260	—	—	dubious
03 55 08.18	23 58 08.7	19.528	18.388	17.863	17.393	—	—	dubious

Table E1. Near-infrared (*ZYJHK*) photometry for 16 candidates selected from the (*J* − *K*, *J*) CMD and recovered in the optical surveys (INT+CFHT). This table lists the equatorial coordinates (in J2000), infrared magnitudes, PMs, and membership status of each object. Only one source is likely to be a Pleiades member, two are classified as photometric non-member (PM_NM), and the remaining are likely to be false detection (“dubious”) after examination of the finding charts (note that none lie within a circle of radius 25 mas/yr centered on the Pleiades mean motion, making their membership highly improbable).

R.A.	Dec.	<i>J</i>	<i>H</i>	<i>K</i>	$\mu_{\alpha} \cos \delta$	μ_{δ}	Memb?
03 50 41.16	25 44 24.2	18.776	17.580	16.556	−15.09	−16.61	dubious
03 48 32.69	25 06 05.1	18.539	17.993	17.412	15.82	−12.52	dubious
03 55 57.94	24 41 41.6	18.876	18.173	18.215	−2.06	0.57	dubious
03 55 15.80	24 49 32.6	17.727	17.004	16.698	−8.77	8.36	dubious
03 51 35.09	24 03 36.9	18.247	17.319	16.492	−9.06	−25.29	dubious
03 54 47.20	23 56 48.0	18.845	18.429	18.556	−19.94	10.38	dubious
03 55 45.48	23 51 25.5	18.855	18.416	18.242	2.55	6.91	dubious
03 54 13.41	23 32 22.2	18.674	18.123	18.104	−23.27	−2.48	dubious
03 45 35.26	23 36 39.6	18.898	18.388	18.123	17.73	−5.33	dubious
03 44 19.50	22 39 03.5	18.718	18.342	17.709	−30.75	−16.71	dubious
03 42 43.46	22 38 31.5	18.301	17.735	17.398	−4.35	0.25	dubious
03 43 24.88	22 50 22.2	18.018	17.310	17.065	−0.25	1.76	dubious
03 52 47.30	22 38 42.4	17.579	16.773	15.969	−13.24	0.48	dubious
03 52 54.90	24 37 18.2	18.798	17.742	16.922	14.70	−44.77	Memb
03 40 30.34	25 58 26.0	18.856	18.271	17.747	−28.78	−5.64	PM_NM
03 47 51.19	25 26 57.9	18.200	17.745	17.611	−28.59	−6.22	PM_NM

Table F1. Near-infrared (*ZYJHK*) photometry for 36 photometric low-mass multiple system candidates below $K = 13.5$ mag, corresponding to masses of $0.135 M_{\odot}$ in the Pleiades. This table lists the equatorial coordinates (in J2000), the magnitudes from the GCS, and their PMs. The estimated mass of the primary and the secondary along with the mass ratio (q) are also given for a total mass less than $70 M_{\text{Jup}}$.

R.A.	Dec.	<i>Z</i>	<i>Y</i>	<i>J</i>	<i>H</i>	<i>K</i>	$\mu_{\alpha \cos \delta}$	μ_{δ}	Mass	q
03 41 40.90	25 54 24.1	16.829	15.900	15.173	14.562	14.114	23.78	-37.48	60+60	1.00
03 41 54.16	23 05 04.8	17.336	16.297	15.499	14.912	14.385	10.66	-24.90	55+55	1.00
03 42 07.99	22 39 33.5	18.717	17.397	16.515	15.809	15.191	—	—	40+35	0.87
03 42 59.92	22 42 51.5	16.067	15.267	14.666	14.109	13.708	25.70	-41.46	—	0.00
03 43 34.48	25 57 30.6	16.471	15.605	14.888	14.322	13.896	9.23	-40.49	70+70	1.00
03 44 22.14	23 10 54.8	15.753	15.130	14.495	13.890	13.503	19.04	-39.79	—	0.00
03 44 23.24	25 38 44.9	16.288	15.349	14.692	14.133	13.744	16.08	-28.17	—	0.00
03 44 35.16	25 13 42.8	17.567	16.482	15.651	14.979	14.439	21.14	-39.28	50+50	1.00
03 44 35.90	23 34 42.0	16.224	15.551	14.991	14.369	13.973	21.72	-32.67	—	0.00
03 45 09.46	23 58 44.7	16.820	16.099	15.417	14.830	14.382	30.39	-47.73	65+40	0.62
03 45 31.37	24 52 47.5	17.246	16.226	15.471	14.842	14.329	19.65	-30.23	55+55	1.00
03 45 37.76	23 43 50.1	16.129	15.320	14.710	14.149	13.731	28.02	-41.71	—	0.00
03 45 41.27	23 54 09.8	17.039	16.055	15.345	14.761	14.281	15.29	-42.72	70+40	0.57
03 45 50.66	24 09 03.5	17.352	16.451	15.692	15.060	14.569	17.66	-53.57	60+35	0.58
03 46 02.52	23 45 33.2	18.077	17.254	16.460	15.458	15.012	—	—	40+40	1.00
03 46 03.75	23 44 35.6	18.074	17.137	16.410	15.528	15.040	—	—	40+40	1.00
03 46 08.02	23 45 35.5	18.787	17.829	16.857	15.832	15.324	—	—	35+35	1.00
03 46 10.23	21 52 55.8	16.114	15.233	14.572	13.948	13.547	36.60	-41.94	—	0.00
03 46 22.25	23 52 26.6	17.013	16.179	15.526	14.879	14.440	16.52	-39.19	65+40	0.65
03 46 26.09	24 05 09.5	16.660	15.824	15.127	14.561	14.097	17.99	-40.76	60+60	1.00
03 46 27.10	21 48 22.6	19.764	18.557	17.387	16.557	15.845	—	—	30+30	1.00
03 46 29.11	22 59 47.7	99.999	18.992	17.740	16.768	15.924	—	—	—	0.00
03 46 40.94	22 22 38.2	19.193	18.048	16.910	16.151	15.495	—	—	35+30	0.86
03 46 48.56	23 09 57.6	16.434	15.709	15.087	14.515	14.078	20.25	-36.11	—	0.00
03 46 50.03	24 00 23.6	17.295	16.335	15.594	14.987	14.502	18.70	-36.10	60+40	0.62
03 46 51.82	23 23 09.4	19.574	18.324	17.182	16.399	15.647	—	—	30+30	1.00
03 47 02.35	23 32 36.0	15.568	14.861	14.294	13.715	13.320	20.44	-42.56	—	0.00
03 47 11.79	24 13 31.3	16.182	15.444	14.805	14.234	13.860	9.97	-28.34	—	0.00
03 48 04.67	23 39 30.2	16.964	15.939	15.294	14.683	14.256	21.59	-29.33	65+50	0.77
03 48 31.52	24 34 37.3	19.163	17.784	16.727	15.964	15.343	18.05	-39.05	35+35	1.00
03 50 13.39	23 59 29.8	20.404	19.093	17.845	16.892	16.205	—	—	30+20	0.67
03 51 38.96	24 30 44.8	18.723	17.316	16.408	15.702	15.148	18.71	-41.66	40+35	0.87
03 52 51.79	23 33 48.0	15.881	15.353	14.807	14.114	13.761	21.92	-43.64	—	0.00
03 53 23.13	23 19 20.4	17.768	16.798	15.963	15.327	14.818	—	—	50+35	0.70
03 55 12.61	23 17 37.3	17.758	16.765	15.962	15.330	14.835	—	—	50+35	0.70
03 55 27.06	25 14 45.8	16.048	15.299	14.643	14.046	13.659	22.98	-39.83	—	0.00